

KATHRIIN UTT

Metal Oxide Mesostructures
for Optical Applications



KATHRIIN UTT

Metal Oxide Mesostructures
for Optical Applications



This study was carried out at the Institute of Physics, University of Tartu.

The dissertation was admitted on 22.02.2016 in partial fulfilment of the requirements for the degree of Doctor of Philosophy in materials science, and was allowed for defence by the Scientific Council on Materials Science of the University of Tartu.

Supervisors: Dr. Ilmo Sildos
Institute of Physics, University of Tartu, Estonia

Dr. Sven Lange
Institute of Physics, University of Tartu, Estonia

Dr. Tanel Tätte
Institute of Physics, University of Tartu, Estonia

Opponents: Dr. Krisjanis Smits
Laboratory of Solid State Radiation Physics,
University of Latvia, Riga

Defence: April 28, 2016 at University of Tartu, Estonia

This work was supported by the following agencies and foundations: Graduate School “Functional materials and technologies” (European Social Fund project 1.2.0401.090079); “Mesosystems: Theory and Applications” (TK114); ERDF projects “Carbon Nanotube Reinforced Electrospun Nano-fibres and Yarns” (3.2.1101.12-0018) and “Efficient plasmonic absorbers for solar cells” (3.2.1101.12-0023).



ISSN 2228-0928
ISBN 978-9949-77-065-6 (print)
ISBN 978-9949-77-066-3 (pdf)

Copyright: Kathriin Utt, 2016

University of Tartu Press
www.tyk.ee

CONTENTS

LIST OF PUBLICATIONS INCLUDED IN THE THESIS	7
AUTHOR'S CONTRIBUTION	7
OTHER PUBLICATIONS OF THE DISSERTANT	8
1. INTRODUCTION	9
2. AIM OF THE WORK	11
3. OVERVIEW OF ZrO ₂ PREPARATION	12
3.1 ZrO ₂ as an optical (ceramic) material	12
3.2 Rare earth ions as optical impurities in metal oxide matrix	13
3.3 Sol-gel technology	14
3.3.1 Introduction and general principle of sol-gel chemistry	14
3.3.2 Zirconium alkoxides as precursors	16
3.3.3 Preparation of optical oxide materials by sol-gel method	17
4. ZrO ₂ NANOCRYSTALLINE POWDERS	18
4.1 Introduction	18
4.2 Sample preparation	18
4.3 Results and discussion	19
4.4 Conclusions	22
5. ZrO ₂ MICROROLLS	23
5.1 Introduction	23
5.2 Formation of microrolls	24
5.3 Results and discussion	25
5.4 Conclusions	28
6. SILICA/ZIRCONIA FIBRES	29
6.1 Introduction	29
6.2 Material preparation	29
6.3 Results and discussion	30
6.4 Conclusions	31
7. YSZ MICROTUBES	32
7.1 Introduction	32
7.2 Material preparation	33
7.3 Results and discussion	34
7.4 Applications	37
7.5 Conclusions	38
8. SUMMARY	39
9. SUMMARY IN ESTONIAN	40
10. ACKNOWLEDGEMENTS	41
11. REFERENCES	42

12. PUBLICATIONS	47
CURRICULUM VITAE	83
ELULOOKIRJELDUS	85

LIST OF PUBLICATIONS INCLUDED IN THE THESIS

- I. L. Puust, V. Kiisk, **K. Utt**, H. Mändar, I. Sildos, (2014). Afterglow and thermoluminescence of ZrO₂ nanopowders. *Central European Journal of Physics*, 12(6), 415–420.
- II. **K. Utt**, S. Lange, M. Järvekülg, H. Mändar, P. Kanarjov, I. Sildos, (2010). Structure and optical properties of Sm-doped ZrO₂ microrolls. *Optical Materials*, 32(8), 823–826.
- III. **K. Utt**, M. Part, T. Tätte, V. Kiisk, M. G. Brik, A. A. Chaykin, I. Sildos, (2014). Spectroscopic properties of Eu-doped Y-stabilized ZrO₂ microtubes. *Journal of Luminescence*, 125–128.
- IV. T. Tätte, M. Part, R. Talviste, K. Hanschmidt, **K. Utt**, U. Mäeorg, I. Jögi, V. Kiisk, H. Mändar, G. Nurk, P. Rauwel, (2014). Yttria stabilized zirconia microtubes for microfluidics under extreme conditions. *RSC Advances*, 4(34), 17413–17419.

AUTHOR'S CONTRIBUTION

Author's contribution to each research paper is given in the list below.

- I. The author was responsible for preparing the samples by using the sol-gel method, for the thermal treatment of prepared samples and for measuring of the Raman spectra.
- II. The author was responsible for the thermal treatment of the samples and participated in all measurements and data analysis. The author participated in the manuscript preparation.
- III. The author participated in all measurements, in data analysis and in the manuscript preparation.
- IV. The author participated in the fluorescence decay kinetics measurements. The author was responsible for the micrographs of light propagation in microtubes. The author participated in the manuscript preparation.

OTHER PUBLICATIONS OF THE DISSERTANT

1. V. Kiisk, L. Puust, **K. Utt**, A. Maaros, H. Mändar, E. Viviani, F. Piccinelli, R. Saar, U. Joost, I. Sildos, (2016). Photo-, thermo- and optically stimulated luminescence of monoclinic zirconia. *Journal of Luminescence*, 174, 49–55.
2. M. Eltermann, K. Utt, S. Lange, R. Jaaniso, (2016). Sm³⁺ doped TiO₂ as optical oxygen sensor material. *Optical Materials*, 51, 24–30.
3. V. Kiisk, A. Tamm, **K. Utt**, J. Kozlova, H. Mändar, L. Puust, J. Aarik, I. Sildos, (2015). Photoluminescence of atomic layer deposited ZrO₂:Dy³⁺ thin films. *Thin Solid Films*, 583, 70–75.
4. T. Dedova, I. Gromyko, M. Krunks, V. Mikli, M. Grossberg, I. Sildos, I.; **K. Utt**, R. Vessart, T. Unt, (2015). Spray pyrolysis deposition and characterization of highly c-axis orientated hexagonal ZnS nanorod crystals. *Crystal research and technology*, 50(1), 82–95.
5. D. Klauson, I. Gromyko, T. Dedova, N. Pronina, M. Krichevskaya, O. Budarnaja, I. Oja Acik, O. Volobujeva, I. Sildos, **K. Utt**, (2015). Study of photocatalytic activity of zinc oxide nanoneedles, nanorods, pyramids and hierarchical structures obtained by spray pyrolysis. *Materials Science in Semiconductor Processing*, 31, 315–324.
6. T. Dedova, M. Krunks, I. Gromyko, V. Mikli, I. Sildos, **K. Utt**, T. Unt, (2014). Effect of Zn:S molar ratio in solution on properties of ZnS thin films and formation of ZnS nanorods by spray pyrolysis. *Physica Status Solidi A – Applications and Materials Science*, 211(2), 514–521.
7. U. Joost, A. Saarva, M. Visnapuu, E. Nõmmiste, **K. Utt**, R. Saar, V. Kisand, (2014). Purification of titania nanoparticle thin films: Triviality or a challenge? *Ceramics International*, 40(5), 7125–7132.
8. U. Joost, R. Pärna, M. Lembinen, **K. Utt**, I. Kink, M. Visnapuu, V. Kisand, (2013). Heat treatment and substrate dependent properties of titania thin films with high copper loading. *Physica Status Solidi A – Applications and Materials Science*, 210(6), 1201–1212.
9. V. Kiisk, S. Lange, **K. Utt**, T. Tätte, H. Mändar, I. Sildos, (2010). Photoluminescence of sol-gel-prepared hafnia. *Physica B: Condensed Matter*, 405, 758–762.

1. INTRODUCTION

Transition metal oxides TiO_2 , ZrO_2 and HfO_2 , which exist in the form of amorphous glasses, polycrystalline ceramics and crystals, have a list of valuable properties including high refractive index, high hardness, high mechanical and chemical stability, nonlinear optical properties, etc. A broad variety of possible applications including construction materials, thermo-electrical isolation layers, electronics components, pigments, etc., are based on these properties. In high-tech industry, especially in optical devices, natural minerals cannot directly be applied due to insufficient purity and structural homogeneity. In many cases specific dopants are also required at known concentrations. For these reasons controllable methods for synthesis of metal oxides with controlled phase composition and morphology are requested [1].

In practical applications, particularly in optics, not only the physical and chemical properties of the material, but also its dimensions and shape are important and play a role in the overall functionality. Hence, it is not only important to tailor the chemical composition, but also the geometry of the material. A lot of effort is put into developing synthetic methods that allow preparation of highly homogeneous and optically active materials with specific geometry both on nano- and microscale. One such method that fulfils latter requirements rather well is sol-gel technology [2, 3]. By using sol-gel, when the purpose of the synthesis is to get materials in structurally homogeneous 3D form, the process is often started by growing nanoscale metal oxide particles (sols) in the liquid phase. In the next step, the particles are let to form solid 3D particle network (gel) over the whole volume of the liquid. Solvents (liquid phase) are functional in such synthesis mostly in order to separate solid sol particles from each other. However, after the gelation process has occurred, the solvent has to be removed from the gel. This is normally achieved by aging and mild thermal treatment. Obtained much more dense gels, which are free of the liquid phase, are known as xerogels.

Depending on the synthesis parameters, combined with appropriate mechanical processing methods, the final mesostructured material can have many different functional shapes. The wet chemistry (synthesis of sol particles) and mechanical processing (shaping of the sol particles prior to or during the gel formation) of the material are mostly carried out at room temperature. Thermal treatment is applied as post processing for the purpose of additional purification, densification, and crystallization of materials. Sol-gel method can be used, for example, for synthesis of nanocrystalline powders that can be further processed into different shapes by high-temperature powder sintering methods, thin film structures for different protective or optical coatings, amorphous or polycrystalline glass-ceramic nano- or microfibres for catalytic or sensor applications, and even bulk glasses for laser optics [4]. One of the advantages of preparation of metal oxides from sols is the easiness to incorporate dopants and other materials in small quantity to the host material.

The main requirement here is solubility of dopant in the initial sol as dopant is usually added during the early stage of the synthesis. Such flexibility of chemical composition is very important as dopants are used to adjust and even create functional properties like electrical conductivity, mechanical stability, luminescent properties, etc., in the final material. The sol-gel technique is becoming one of the cheapest and most versatile methods for fabrication of components for integrated optics [5]. The list of practical applications of the obtained materials also includes active components in light sources like light emitting diodes and lasers.

In the present thesis the main attention is paid to controllable syntheses of nanostructured ZrO_2 with different defined morphologies (powders, microrolls, fibres and tubes). The materials are post-treated and possibilities of applying them mainly as optical materials are proposed. In addition peculiarities and photoluminescence features introduced by the RE^{3+} doping and practical use of the latter for detecting materials' crystallographic phase are investigated.

Table 1: A short list of prepared mesostructured materials

Prepared structure	composition
Nanocrystalline powder	ZrO_2
microrolls	$ZrO_2:Sm^{3+}$
fibres	1) $ZrO_2(6.5\%)-SiO_2:Sm^{3+}$ 2) $ZrO_2(30\%)-SiO_2:Sm^{3+}$
microtube	YSZ:Eu ³⁺

2. AIM OF THE WORK

The goal of the thesis is to develop a synthetic route for preparation of meso-structured nanocrystalline ZrO_2 and similar oxides with good optical quality with different morphologies (powders, microrolls, fibres, and tubes). It is also demonstrated that different optically active RE^{3+} ion dopants could be incorporated into the host materials to enhance their functionality in different applications. To characterize the quality of the materials, comprehensive study of the phase structure is performed by using PL and Raman methods.

Following tasks were set to achieve the general goals:

- To establish the conditions of sol-gel synthesis and temperature treatments necessary for preparation of oxide materials with various morphologies.
- To investigate the influence of the phase structure of the materials to their microstructure and optical properties.
- To elaborate the methods for preparing luminescent RE-doped metal oxides.
- To use RE^{3+} ions as optical probes for the study of the evolution of crystalline structure formation in studied materials during the temperature treatment.

3. OVERVIEW OF ZrO₂ PREPARATION

3.1 ZrO₂ as an optical (ceramic) material

Zirconium oxide (zirconia, ZrO₂) ceramics are important technological materials that have found use in many applications, including due to wide range on useful properties. Zirconia has high refractive index, optical transparency, chemical and photochemical stability, and thermal isolating properties. Zirconia also has low phonon energy and relatively high band-gap (> 5 eV), that make it an attractive host for RE³⁺ (rare earth) ion dopants. Properly doped materials show high luminescence yield [6, 7].

Nanoceramic zirconia has also found use as an optical coating material (such as antireflective or abrasion resistant layers) [8], solid state electrolyte in high temperature solid oxide fuel cells (SOFC) [9], thermal barrier coating in engines and gas turbines [10], oxygen sensor [11], and as a scintillator dosimeter for ionizing radiation [12]. Zirconia is also a biocompatible material and has found use in dental implants [13, 14]. Many RE³⁺ doped zirconia based ceramics have been proposed for use as luminescent phosphors in displays and lighting devices and even in laser sources [15].

At normal pressure, pure zirconia can exist in three well-known polymorphic crystal phases: monoclinic (C_{2h}), tetragonal (D_{4h}), and cubic. At room temperature, the only stable polymorph is the monoclinic phase, the tetragonal structure becomes thermodynamically stable above ~1170 °C, and the cubic above ~2370 °C [16]. If the temperature decreases, the cubic structure transforms back to tetragonal and monoclinic structures. This transformation is destructive for the material due to the difference in size of tetragonal and monoclinic volume cells (volume increase of 3–5 % upon the transition from tetragonal to monoclinic) causing evolution of cracks in the material [17].

Technologically, the high-temperature cubic and tetragonal phases are found to be more useful, which for a lot of efforts are put into research to stabilize those phases at low temperatures. There are two main ways to stabilize the metastable tetragonal and cubic phases at room temperature. Firstly, the most common method is to incorporate di- or trivalent cationic species such as Mg²⁺, Ca²⁺ or Y³⁺ into the zirconia matrix, where the structure is stabilized by the created defects. For the tetragonal phase usually 5–10% additive is used, and for the cubic phase ~ 20% [16]. Alternatively, the metastable phases can be stabilized by the size of the crystallites. It is found that pure zirconia can be stable in the tetragonal phase at room temperature if the crystallite size is smaller than about 30 nm, where the stabilization occurs due to the high surface energy [18].

There are many wet chemistry methods to synthesise zirconia in fine-powder form, precipitation from zirconium alkoxides or salts [19], hydrothermal synthesis [20, 21], or sol-gel method [22]. To produce zirconia thin films or coatings, different chemical or physical vapour deposition methods like atomic layer deposition (ALD) and pulsed laser deposition (PLD) are widely used [23].

Sol-gel method is used for the purpose in combination with spin-coating, dip-coating, or spray-coating. Sol-gel technique seems to be the best option to synthesise highly functional structures with homogeneous composition [24]. Attention should be paid to differences in crystal size, amount of defects, porosity and residual –OH groups and additives inside the material as factors that can lead to final materials with different properties [25].

3.2 Rare earth ions as optical impurities in metal oxide matrix

The rare earth (RE) elements occupy a special place in the periodic table of elements, due to a particular way their 4f electron shell is filled. They are in the fifth period after lanthanum from cerium ($Z=58$) to lutetium ($Z=71$); with increasing the atomic number by unity in this group the number of 4f electrons increases from 1 (Ce) to 14 (Lu). When RE elements are incorporated into solids, they are stabilized in the triply charged states (in the vast majority of cases). However, other oxidation states such as +2 and +4 can also be met occasionally. When RE ions are ionized, their 5d and 6s electrons have to be removed, whereas the 4f shell is kept to be partially filled. Coulomb interaction between 4f electrons gives rise to a large number of energetic states in the infrared, visible, and ultraviolet spectral ranges. Many of those energy levels can be linked by the electric dipole transitions, which open numerous opportunities for application of these ions in optoelectronic devices. A special feature of those elements is that the optically active 4f electrons of RE ions are shielded by the completely filled 5s and 5p electron shells. Due to this fact, the 4f optical electrons of RE ions in solids only weakly interact with the crystal lattice surrounding, which leads to very minor changes of the characteristic emission/absorption transitions of RE ions from one host to another. If the influence of neighbouring ligands on the energetic structure of RE ions can be neglected, their energy levels can be characterized by the L, S, J quantum numbers, as for free ion. A weak interaction between the 4f electrons and the crystalline field splits the free ion's levels producing very well resolved Stark structure in the optical spectra, which, as it was mentioned above, varies slightly (compared with the 3d ions, for example) from host to host. The number of split levels is determined by the local symmetry around an RE ion.

The 4f-4f electronic transitions in the spectra of trivalent RE ions are parity forbidden and appear as sharp lines with very weak phonon sidebands. Electronic transitions in spectra of RE ions in solids can be broadened homogeneously or inhomogeneously. The inhomogeneous broadening originates from local variations in surrounding of each optical centre, while the homogeneous broadening is determined by the lifetime of the excited electronic level. Every homogeneous transition produces a Lorentzian-shaped line giving its contribution to the inhomogeneously broadened line (Gaussian in shape).

For the Eu^{3+} in solids, the ground state ${}^7\text{F}_J$ and excited electronic states are split depending on the local symmetry [26], and optical transitions from the

excited 5D_0 state to the ground state multiplets are first of all spin-forbidden, as $\Delta S=1$. In the case of ZrO_2 , the crystal lattice can be monoclinic, tetragonal, or cubic. The $^5D_0-^7F_2$ optical transition observed at 612 nm is an electric dipole transition, while the $^5D_0-^7F_1$ transition at 590 nm is a magnetic dipole transition. The ratio of intensities of these electric and magnetic transitions is a measure of the site symmetry for Eu^{3+} ion (Eu can be viewed as a local probe of symmetry [27]). Higher symmetry around the Eu^{3+} ion leads to the lower e/m ratio [28].

3.3 Sol-gel technology

3.3.1 Introduction and general principle of sol-gel chemistry

Sol-gel technology is a wet chemical approach in materials synthesis, based on nanocolloidal dispersions of solids in liquid phase (sols) as precursors that are let to form three dimensional networks over whole volume of liquid phase (gels). The method is called “sol-gel” due to its most critical and characteristic step: transition of randomly oriented sols into structured gels. However, in reality, the scope of the technologies is far broader, consisting the steps of sols formation, removal of liquid phase from resultant material, sintering of materials for the purpose of densification, crystallization and removal of residual materials. The method is most usually been applied to prepare nano- and microcrystalline metal oxide materials in different geometrical shapes: powders, films, fibres, monoliths, aerogels etc. from metal-oxo-alkoxides in liquid phase as most common sol-precursors [2, 29]. The shaping is done by combining the material synthesis with various mechanical methods like spin-coating to get thin films or electrospinning to get fibre mattes.

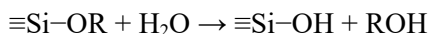
Sol-gel method in general is a versatile and a low-cost method that allows low-temperature synthesis of highly homogeneous and complex materials. It is easy to dope and vary the composition of the materials by adjusting the concentrations of the starting solutions, meaning that there is no need for complex preparation methods or extreme conditions (like high-temperature powder sintering technologies or ion implantation methods for doping). The method also has some disadvantages, like: the more complex precursor materials can be expensive, the precursor materials can be highly sensitive to moisture leading to the need for careful handling, the removal of solvents and organic residues from prepared gel can be difficult, and upon the sol-gel transition followed by subsequent heat-treatment rather large volume shrinkage of materials can occur.

Sol-gel chemistry as a chemical background of formation of sols and sol-gel transition process is usually illustrated using an example of different silicon alkoxides (like tetraethyl ortosilicate (TEOS, $Si(OC_2H_5)_4$) where highly cross-linked inorganic polymeric network that is considered as gel is formed via hydrolysis and condensation reactions. Hydrolysis, followed by partial condensation leads to a dispersion of colloidal particles called sol; on a further condensation the sol particles form an inorganic interconnected network of particles

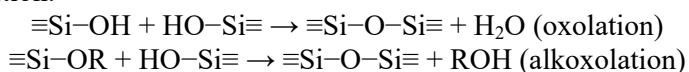
called gel. The gel is porous in nature and still includes a continuous liquid phase.

The hydrolysis reaction between the metal alkoxide and water leads to formation of a silicon hydroxide and respective alcohol. The hydrolysis reaction is followed by a condensation reaction, either by oxolation, where M-O-M bonds are formed by reaction between two hydroxylated metal species, or alkoxolation, where the M-O-M bonds are formed by reaction between a hydroxylated silicon species and a non-hydrolysed silicon alkoxide [30]. The only side products of these reactions are water molecules, that are used for further hydrolysis, and alcohol. Because the different reactions happen simultaneously it would be difficult to fully control the process.

Hydrolysis:



Condensation:



The course of hydrolysis reaction is mostly affected by the molar ratio of water to alkoxide. This ratio determines the course of the hydrolysis and condensation reactions and thus determines the final shape of the obtained hydroxides and oxides. Because of the strong sensitivity to changes of water concentration during the sol-gel transformation, an uncontrolled hydrolysis is a big problem that leads to the formation of intermediate Si/alkoxide species with unknown shapes and sizes [31]. Therefore the anhydrous solvents should be used, and the synthesis should be carried out in dry atmosphere conditions.

For catalysing the linear species formation process, mineral acids are used (mostly HCl, HNO₃). The acid catalyses the elimination of ROH and the formation of OH-groups at the ends of chains during the hydrolysis step, thus resulting in the formation of linear species. At high acid concentrations the condensation process is considerably slowed down and leads to formation of a (uniform) gel. At low acid concentrations, precipitate is formed.

The products of the sol-gel synthesis are most likely amorphous. To obtain crystalline materials, a thermal post-treatment should be applied. Prior to the thermal treatment, the material is dried at a lower temperature, so that the alcohol and water trapped in the gel network can evaporate, thus enabling the forming of xerogels. The following thermal treatment is carried out at higher temperatures. The residual carbon can be eliminated at temperatures from 300 °C to 400 °C. At temperatures higher than 400 °C, the oxide crystallisation can take place. Most importantly, as an advantage of the method, the formed oxide materials retain their geometrical shape obtained prior to the gelification, as e.g. thin film, bulk piece, or fibre.

3.3.2 Zirconium alkoxides as precursors

In contrast to the hydrolysis of non-metal silicon alkoxides, $\text{Si}(\text{OR})_4$, the hydrolysis of metal alkoxides, $\text{M}(\text{OR})_n$, is an extremely quick process. The chemical reactivity of alkoxides towards hydrolysis increases in the order of $\text{Si} < \text{Sn} < \text{Ti} \ll \text{Zr}, \text{Al}$ (Zr alkoxides react readily with water molecules and are thus very sensitive to atmospheric moisture).

It was supposed, in analogy with the silicon alkoxides, that the metal alkoxides follow the same route of firstly forming hydroxo-alkoxide species through hydrolysis (like $\text{M}(\text{OR})_3\text{OH}$) that can then hydrolyse further or undergo condensation through formation of oxo- or hydroxo-bridges. But for homometallic alkoxides of, for example, titanium and zirconium the addition of small amounts of water does not proceed in formation of intermediate hydroxide species, but through the one-step hydrolysis-condensation transformation well-defined oligonuclear oxo-alkoxide species are formed. This transformation occurs due to the restructuring of precursor molecules to achieve the coordination equilibrium. The formed oxo-alkoxide species subsequently form larger aggregates with a crystalline or at least short-order organized core and a shell consisting of a hydrated amorphous oxide and of stabilizing ligands (referred to by V.G. Kessler as Micelles Templated by Self-Assembly of Ligands, MTSAL) [32, 33].

The average complexity and molecular weight of those species formed in the initial hydrolysis process depends mostly on the water-to-alkoxide ratio. Excess amount of water, more than a mole per a mole of alkoxide, results in cross-linking of the particles forming gel network or individual particles in the form of amorphous precipitates that still contain residual alkoxide groups [31].

An agglomeration of particles obtained by the alkoxide hydrolysis is a big problem because the agglomerated particles cannot be re-dispersed due to oxolation and alkoxolation reactions [34]. So, the hydrolysis of concentrated solutions with a high alkoxide-to-water ratio leads to polydisperse precipitates. It is complicated to obtain uniform and dense submicron particles. To avoid the agglomeration, highly dilute and homogeneous solutions should be used, which means that high yields of precipitate with uniform dispersion cannot be achieved. To overcome this problem, additional molecules acting as agglomeration preventing agents should be introduced to the solution like acetylacetone.

In comparison with $\text{Si}(\text{OR})_4$, the higher coordination number of metals in their alcoholic derivatives leads to growth of oligonuclear metal-oxo-alkoxide clusters already prior to their further hydrolysis. Therefore even commercially available metal alkoxide precursors are not mononuclear, for example zirconium n-propoxide and n-butoxide contain up to ~20 and ~35% of $\text{Zr}_3\text{O}(\text{OR})_{10}$, respectively [35]. These processes finally result in more complicated structures of metal alkoxides hydrolysis products compared to silicon alkoxides.

3.3.3 Preparation of optical oxide materials by sol-gel method

The advantages of sol-gel method over other methods, used for preparation of optically active, rare-earth-activated materials, include flexible doping (with rather high rare earth solubility) and varying the composition. Depending on the chosen synthesis parameters (the amounts of water, catalyst, solvent, and other additives allowing to steer the reaction), different products such as powders, thin films, fibres, aerogels, and bulk glasses can be obtained by using methods such as spin-coating, electrospinning, extrusion, supercritical drying etc. [2, 5].

When preparing thin films, most important parameters are the sol concentration and the precursor viscosity; these can be modified by the amounts of water and solvent added. With dilute solutions, thin films with thicknesses of even less than some tens of nanometres can be produced. Obtaining thick films in the range of micrometres is more difficult because of cracking of the film due to capillary forces caused by the solvent evaporation and the material densification in the process of gelling. The unwanted cracking can be overcome by adding modifiers to the precursor to slow down the processes [36].

Self-standing “bulk” materials can be prepared from precursors with much higher viscosity that help to avoid cracks, or methods such as supercritical drying to avoid capillary forces [37]. Bulk, optically active, and transparent objects can also be made by sintering of nanoparticles with a narrow size distribution [38]. Sol-gel prepared bulk glasses and nanoceramics are usually not that dense as materials prepared by high-pressure-sintering. However, in optics related applications they still have many advantages as very high homogeneity and easiness to prepare them doped by optically active additives. It is noteworthy that preforms for optical cable drawing in industrial scale are made by using sol-gel technology due to the above mentioned reasons [39].

4. ZrO₂ NANOCRYSTALLINE POWDERS

4.1 Introduction

Depending on the material preparation and thermal treatment properties, undoped zirconia can be synthesised as a mixture of tetragonal and monoclinic phases (with a degree of variability), or as a material consisting only of pure monoclinic phase. In the case of undoped zirconia, the tetragonal phase is stabilized by the small size of crystallites [18], meaning that increasing of the thermal treatment temperature decreases the amount of the tetragonal phase in the material.

Monoclinic ZrO₂ has a well-known intense broadband photoluminescence (PL) emission around 490 nm and tetragonal – around 410 nm [40]. That PL emission has so far been attributed to either oxygen vacancies [41-43], or Ti impurity centres in the material [44-46], (all “undoped” zirconia contains trace amounts of metal impurities including Ti).

Many studies have also reported the thermoluminescence (TL) of monoclinic zirconia [42, 46-49], and its potential for dosimetry has been suggested [49]. The PL of zirconia also frequently gives an afterglow emission (persistent luminescence) for hundreds to thousands of seconds [42, 43, 45, 47]. In comparison with many presently used phosphors, ZrO₂ has advantages of a relatively simple structure, of a good mechanical, chemical, and thermal endurance, and of rather simple preparation methods. Moreover, ZrO₂ is also considered being biologically inert and non-toxic, which provides an opportunity to use its afterglow properties, e.g., as autonomously emitting bio-labels in in-vivo medical research [50].

The aim for the first part of the thesis is to prepare a simple ZrO₂ powder and assess usability of its dopant-less pristine form as a persistent luminescence material. An attempt is made to clarify aspects of the origin of persistent PL emission and its storage states.

4.2 Sample preparation

For the powder preparation, firstly a zirconium butoxide (80 wt% in 1-butanol) was dissolved in 1-propanol at a volume ratio of 1:1. Secondly, the obtained solution was added drop-wise under vigorous stirring to a solution of distilled water and hydrochloric acid (0.1%). As a result, a white precipitant formed in the solution, the excess water was decanted, and the obtained material was left to dry at room temperature for several days. The prepared dry powder was divided into several parts that were annealed either at 500, 750, 1000, 1250, or 1500 °C for 2 hours.

The annealed powders were polycrystalline in nature, with crystallite size of 10–40 nm and average particle size of ~300 nm (Figure 1).

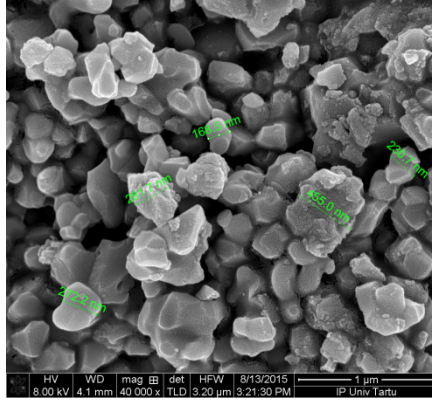


Figure 1: SEM micrograph of ZrO_2 powder annealed at 1250 °C

4.3 Results and discussion

According to the measured XRD spectra (Figure 2), the tetragonal phase is present in a small quantity for samples annealed at temperatures 500 °C (2.8%), 750 °C (0.6%) and 1000 °C (0.3%). Samples annealed at 1250 and 1500 °C are fully monoclinic. The Rietveld analysis gives an average size of tetragonal crystallite for a sample annealed at 1000 °C as 25(3) nm (Table 2), meaning that any additional rise in temperature will grow too big crystallites to be stabilized only by their size, and the material will become fully monoclinic. The phase evolution can also be seen from the measured Raman spectra (Figure 3).

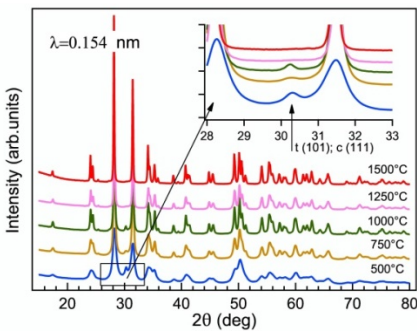


Figure 2: X-ray diffraction patterns of ZrO_2 powders after annealing at different temperatures. The inset shows the strongest reflection of tetragonal (or cubic) phases

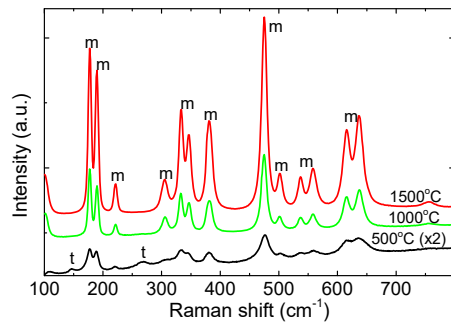


Figure 3: Raman spectra of ZrO_2 powders after annealing at different temperatures. Marked are peaks of tetragonal (t) and monoclinic (m) phases.

Table 2: Average crystallite size for tetragonal and monoclinic phases at different annealing temperatures.

t (°C)	Size of the crystallite (nm)		Tetragonal (%)
	t	m	
500	9(1)	8(1)	2.8
1000	25(3)	33(4)	0.3
1500	–	36(6)	0

Only the samples annealed at temperatures of 1000, 1250 and 1500 °C (with almost pure and pure monoclinic phase accordingly) were found suitable for thermoluminescence and afterglow measurements (no TL or afterglow emissions were detected for samples annealed at 500 °C and 750 °C). For the monoclinic samples, the intrinsic luminescence emission band was centred at 490 nm and the excitation band – at 280 nm (Figure 4). For the samples annealed at 500 °C and 750 °C the PL emission is blue-shifted and is centred at around 410 nm.

Higher annealing temperatures don't only affect the size of the crystallite but also the composition and amount of defects such as oxygen vacancies and Ti impurity centres, which play an important role in ZrO₂ luminescence properties. The overall amount of Ti impurities in the material does not change as a result of annealing, which affects only the ratio of Ti⁺⁴ to Ti³⁺. According to X-ray fluorescence measurements, the content of Ti impurity in the prepared zirconia material was less than 340 ppm.

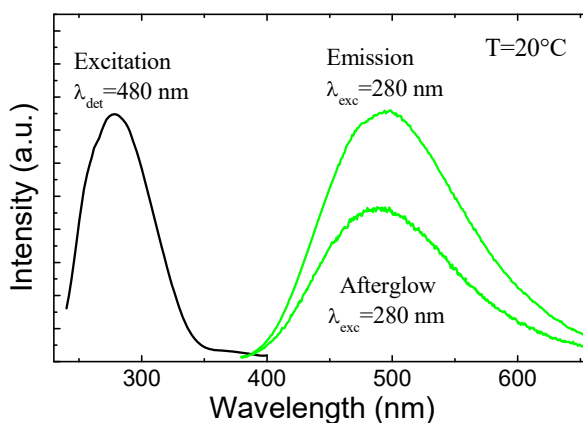


Figure 4: PL emission and excitation spectra of ZrO₂ powder annealed at 1250 °C.

The most intense initial afterglow was obtained from the sample annealed at 1250 °C (Figure 5). The afterglow was observable by eye for up to several minutes. The emission from the sample annealed at 1000 °C was clearly weaker. To identify the origin of the afterglow in the material, the TL glow curves were measured. The powders were charged with 280 nm for 3 min and the glow curves were recorded at a rate of 20 °C/min in the range of -100 °C to 300 °C (Figure 6 and Figure 7). In this range the zirconia powders gave four distinct glow peaks at approximately -35, 5, 110, and 205 °C. The wavelength-resolved TL of a sample annealed at 1250 °C (Figure 6) indicates that there is only a single prevalent luminescence centre.

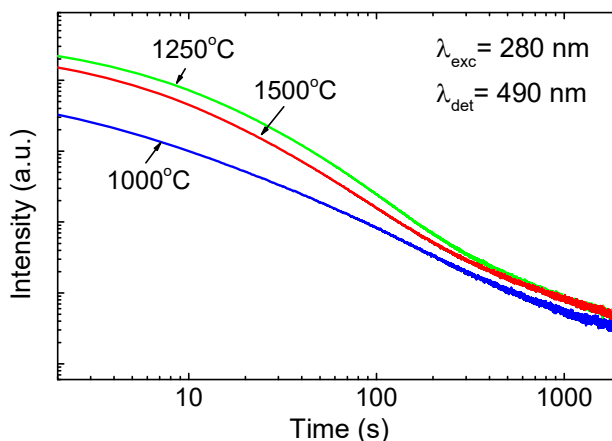


Figure 5: The decay of the PL afterglow of the ZrO₂ powders at room temperature after charging at 280 nm for 3 min. Note that double-log scale is used.

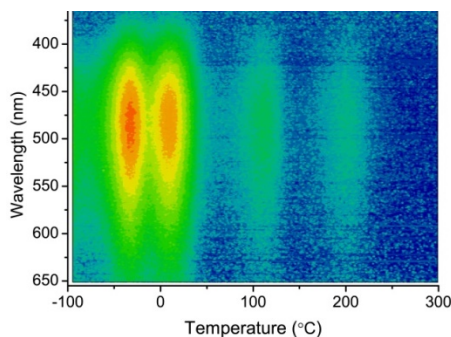


Figure 6: Wavelength-resolved TL of a sample annealed at 1250 °C. Colors are illustrative.

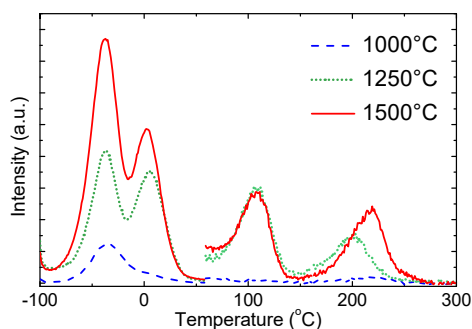


Figure 7: The TL glow curves of ZrO₂ powders recorded at a rate of 20 °C/min after charging at 280 nm for 3 min. The right half of the graph is multiplied by 10 for better visibility of the high-temperature glow peaks.

4.4 Conclusions

Within the frames of the conducted study a set of pure ZrO_2 powder samples were synthesized via sol-gel route. When excited over band-gap (in UV) prepared monoclinic nanocrystalline zirconia powder appears to have a broad intrinsic luminescence band centred at 490 nm. The PL is shown to persist for of several minutes which enable to classify it as an afterglow material.

The wavelength-resolved thermoluminescence recorded in the range of $-100\text{ }^\circ\text{C}$ to $300\text{ }^\circ\text{C}$ reveals four distinct glow peaks, which suggests that ZrO_2 nanopowders contain a single prevalent luminescence centre fed by several higher energy bands. The ZrO_2 occurs to be a promising afterglow material for future modifications and research in the field of persistent luminescence materials.

5. ZrO₂ MICROROLLS

5.1 Introduction

Conventionally the sol-gel process has been successfully used in the preparation of thin films from various precursor materials. On the other hand, thick coatings have always been difficult to prepare. That is because of the stresses caused by the solvent evaporation and densification process causes cracking of the film into smaller segments [51]. By using these processes, unwanted in most cases, and also by slightly modifying the conventional sol-gel process to achieve a gelling gradient in the film layer, formation of microroll structures can be achieved. The rolls are essentially spontaneously rolled-up segments of a gelled material that are formed by the usually unwanted cracking of a (thick) film.

A rolled-up microstructure of metal oxide with a high surface-to-volume ratio could be specially functionalized to be used among other possible uses as a catalyst or a filter material for the removal of harmful airborne contaminants in the industry.

In the following work an attempt is made us utilise the novel approach to prepare luminescent ZrO₂ microrolls (Figure 8), monitor their phase composition via incorporated Sm³⁺ ion PL during thermal annealing and explain key findings about the process.

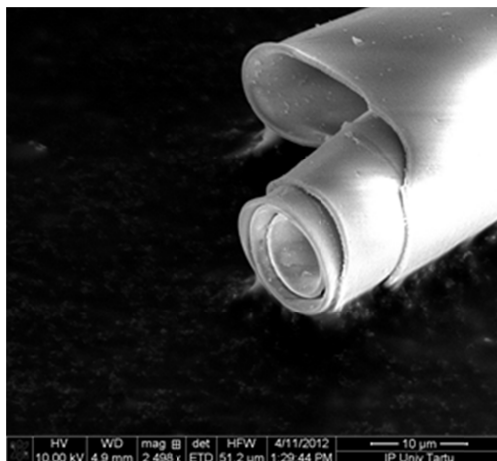


Figure 8: SEM image of a single microroll

5.2 Formation of microrolls

Microrolls were prepared by the controlled hydrolysis of $\text{Zr}(\text{OBU})_4$. Firstly, the zirconium butoxide (as bought, 80wt% in butanol) was further diluted in butanol (to achieve a homogeneous sol after addition of deionized water). Secondly, a solution of butanol, deionized water, hydrochloric acid (HCl), and samarium(III) chloride hexahydrate ($\text{SmCl}_3 \cdot 6\text{H}_2\text{O}$) was prepared (with molar ratio of 4.4 (for both solutions combined) /0.4/0.06/0.005 accordingly to the used amount of alkoxide). The amount of butanol in the second solution was chosen so that the concentration of water in this solution is less than 4%. If the amount of water is higher than that, some of it can remain undissolved and cause an inhomogeneity in the sol formation. HCl was added to the solution to catalyse more linear particle growth in the sol-gel process. Samarium(III) chloride hexahydrate was used as a source of Sm^{3+} ions.

To prepare the partially hydrolysed sol, the water-containing solution was added drop-wise under vigorous stirring to the diluted $\text{Zr}(\text{OBU})_4$. After thorough mixing, a clear solution with low viscosity was obtained. To get a viscous solution suitable for formation of a thick film layer, the excess solvent was removed by evaporation under vacuum condition as the used round-bottomed flask was rotated in a water bath at 80 °C. The same rotational movement was used to cover the inner surface of the flask with an even layer of non-flowing (that's why the partial hydrolysis was used) thick precursor sol film. Next, to achieve the gelling of the top layer of that thick film, a high humidity air (obtained from above the water bath) was introduced into the system. Water molecules from the humid air do not diffuse into the whole sol layer due to the denser gel formation on the upper layer of the film caused by the fast hydrolysis and polymerization. Latter also prevents further diffusion of water and also the solvent evaporation from the unpolymerized under-layer. Subsequently, this also leads to the gradient formation in gelation. Also the spontaneous cracking of the formed film into micrometre-sized segments occurs due to the solvent evaporation from the upper layer (alcohol is also a polymerization process by-product in the alkoxide based sol-gel). If a proper solvent (hexane in this case) is added to the system, the underlying sol layer is dissolved and now freestanding segments of the gel film spontaneously roll up to form microrolls (Figure 9). The rolled structure formation occurs because the gelation gradient causes the top side of the film to shrink more than the other side, producing mechanical stress on one side of the film. The remaining sol is removed by washing the microrolls with several cycles of diluting and decanting.

The formed microrolls are in average 100–300 μm long (depending on the size of the film segments produced by the cracking process) and have a diameter of 10–20 μm ; the thickness of the rolled-up film is in the range of few hundred nanometres (basically the depth of water diffusion into the sol film).

Microrolls prepared by this method are amorphous in nature, thus the thermal treatment have to be used for formation of the crystalline $\text{ZrO}_2:\text{Sm}^{3+}$. The samples used for further studies were annealed step by step at 500, 600, 700, and 800 °C respectively.

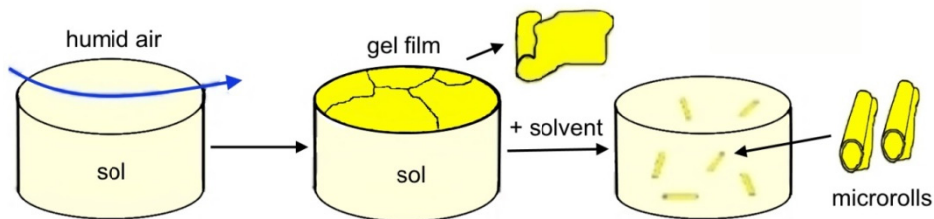


Figure 9: simplified overview of microroll formation

5.3 Results and discussion

To characterize the formation, crystal structure, and optical properties of prepared structures, XRD, Raman, and photoluminescence (PL) spectra were measured after each annealing step, and also scanning electron microscope (SEM) and optical micrographs were taken. It is clearly seen from the taken micrographs (Figure 10) that in the course of annealing process the microrolls tend to break up, causing a lot of debris of smaller oxide fragments, rendering the shape-based functionality of the material useless.

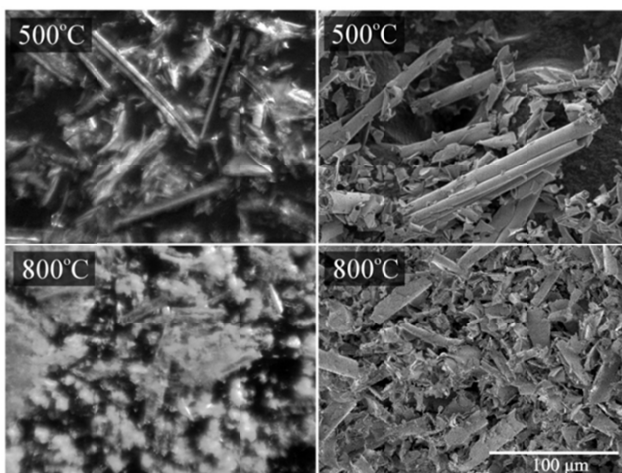


Figure 10: Optical (on the left) and SEM (on the right) micrographs of microroll structures annealed at 500 °C and 800 °C

Knowing that dopant concentration, crystallite size, and temperature can affect the phase composition of ZrO_2 materials, XRD and Raman spectra were measured after each annealing step to characterize the structural changes happening

in the material during the step-by-step annealing process (Figure 11). The measured XRD spectra show that a sample annealed at 500°C contains mostly the metastable tetragonal phase of ZrO₂. Increasing the annealing temperature to 600 °C introduces two additional weak reflections characteristic to monoclinic ZrO₂ phase. The XRD spectra indicate that samples annealed at 700 °C and 800 °C consist mostly of monoclinic phase. The same phase evolution from tetragonal to monoclinic is evident from the measured Raman spectra.

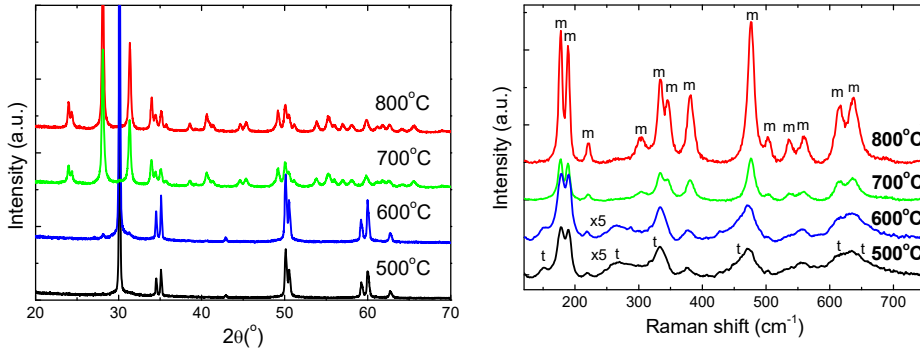


Figure 11: XRD and Raman spectra of ZrO₂ microroll structures showing phase evolution according to the rise in the annealing temperature

With the rise of annealing temperature the average diameter of the crystallites grows; when the temperature drops back to RT, the metastable tetragonal phase structure that is prevalent for the samples annealed at 500 °C and 600 °C is not stable anymore. The crystallite has grown too big, thus the size, the small amount (0.5 mol%) of dopant, and the stress caused by the rolled-up structure do not stabilize it anymore, and it is transformed into the monoclinic phase. But because the primitive cell volume for the monoclinic phase differs from such for the tetragonal phase, the transformation from one to the other causes cracks to form and thus breaks up the microroll structure, as can be seen clearly from the optical and SEM images taken of samples annealed at different temperatures (Figure 10).

The photoluminescence of dopant Sm³⁺ was also used to investigate the changes in crystal structure of zirconia microrolls. Laser excitation at wavelengths of 473, 405, 250, 235, and 210 nm was used. Firstly, under conditions of direct excitation at 473 nm (Figure 12), the PL emission intensity for samples annealed at 500 °C and 600 °C was very weak, but increased many orders of magnitude after annealing at 700 °C. The fine structure of samarium ion spectra for the samples annealed above 700 °C indicates formation of monoclinic zirconia [52, 53], in accordance with XRD and Raman measurements.

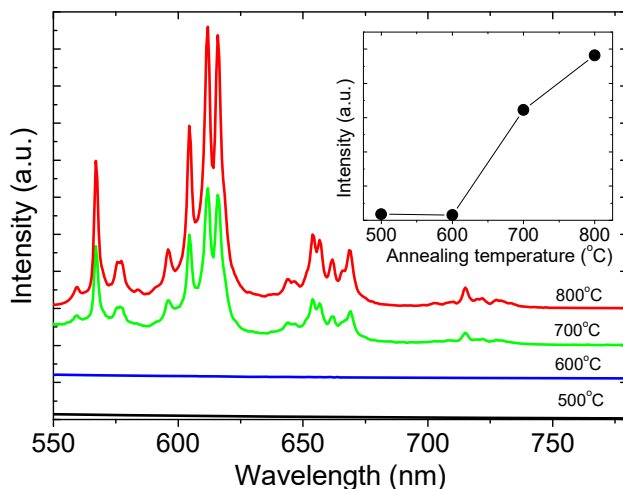


Figure 12: Development of Sm^{3+} PL emission during the annealing cycle from 500 °C to 800 °C under direct photoexcitation at 473 nm. Insert: the integral emission intensity.

As the PL emission of Sm^{3+} ions under direct excitation at 473 nm was very weak, and also did not give any information about the crystal structure for samples annealed at lower temperatures, the emission was further investigated under different excitation energies, allowing to probe the phase composition of microrolls at different depths from the surface. The photon energy of the 405 nm excitation is too low to be absorbed by the zirconia matrix and therefore gives information from the “bulk” of the material. The increasing of the excitation energy from 405 to 210 nm also increases the absorption, allowing to probe only the surface of the crystallites (Figure 13).

For the samples annealed at 500 °C and 600 °C the bulk-material PL spectrum of Sm^{3+} shows only a weak defect-related broadband emission. Moving closer to the surface of the crystallites, a samarium spectrum characteristic to a mixed environment of tetragonal and monoclinic is observed, and when the excitation is confined only to the surface the spectrum of samarium ion in tetragonal phase is prevalent. For the samples annealed at 700 °C and 800 °C no changes in spectral features are observed regardless of the excitation wavelength. The spectral shape for these samples refers to a samarium ions in a monoclinic zirconia surrounding.

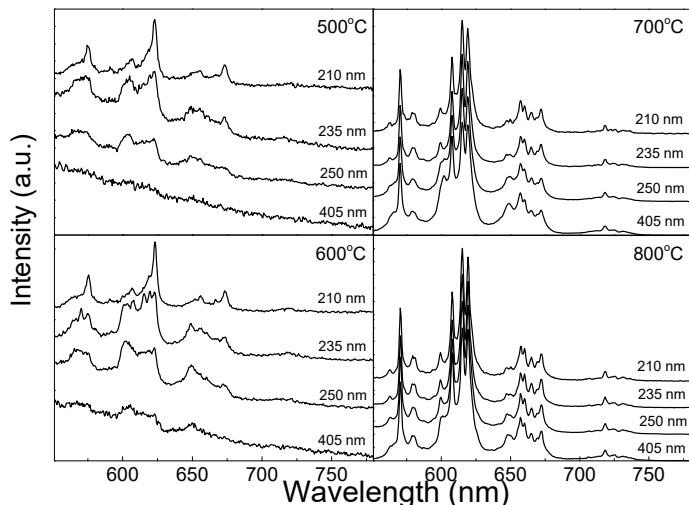


Figure 13: Probing the crystal structure of the microrolls via PL emission spectra of Sm³⁺ ions. The excitation wavelengths 405, 250, 235, and 210 nm correspond to progressively shorter absorption depths. The spectra are normalized.

If the rolled-up structure is desirable, the material in this form should not be annealed (in this case the material will not be an oxide). If good luminescent properties are needed, the material should be annealed at temperatures of at least 700 °C and over. But to get a material with a good crystalline oxide structure, good luminescent properties, and in a rolled-up shape, the stabilization of tetragonal phase is needed.

5.4 Conclusions

A metal oxide material can be shaped into a functional rolled-up microstructure due to the unwanted effect of film cracking and the gelation gradient occurring during the formation of a thin layer, when the material is prepared by the sol-gel reaction of metal alkoxide with water. Doping the precursor material with RE³⁺ ions (e.g. Sm³⁺) adds luminescent properties, and incorporated ions acts as a structural probe giving information about the crystal structure of microrolls. During the annealing process, the unstabilized zirconia is transformed from a metastable tetragonal to a stable monoclinic phase. This transformation leads to the destruction of the roll structure. To avoid the destruction of formed microstructures during the high-temperature annealing process needed to obtain an optically active oxide material, a stabilizing additive should be used.

6. SILICA/ZIRCONIA FIBRES

6.1 Introduction

Recently, rare-earth-doped silica-based binary-oxide systems like silica/hafnia, silica/zirconia, silica/stannia have been studied with the aim to develop a transparent nanoceramics containing emitting RE^{3+} ions located in a crystalline surrounding for improved emission characteristics. The sol-gel method, which allows a high control over homogeneity and composition, can also be used for creating such materials [54]. The nanocrystalline inclusions are obtained via self-formation in the silica host during the high-temperature annealing process [55].

The goal of this investigation was to apply the sol-gel technique in developing fibrous wave-guiding structures based on the zirconia doped with RE^{3+} ions in a silica matrix. Optical and structural properties of pure and rare-earth-doped samples were evaluated by using the luminescence- and Raman spectroscopies and the XRD analysis.

6.2 Material preparation

Samples with two different zirconia concentrations of 6.5 and 30% were made by using the controlled hydrolysis of $Si(OEt)_4$ (tetraethyl ortosilicate, TEOS) and $Zr(OBu)_4$. The concentration of Sm^{3+} was 1%.

For the fibres containing 6.5% of ZrO_2 , firstly the zirconium butoxide (as bought, 80 wt% in butanol) was further diluted in butanol (with molar ratio of 10 for the used amount of alkoxide), and then added dropwise to $Si(OEt)_4$ under stirring. Secondly, a solution of methanol, distilled water, hydrochloric acid (HCl), and samarium(III) chloride hexahydrate ($SmCl_3 \cdot 6H_2O$) was prepared (with molar ratio of 10/1/0.01/0.01 accordingly to the used amount of both alkoxides combined).

For the fibres containing 30% of ZrO_2 , firstly $Zr(OBu)_4$ was further diluted in butanol (with molar ratio of 10 for the used amount of alkoxide) and then added dropwise to $Si(OEt)_4$ under stirring. Secondly, a solution of distilled water (molar ratio of 0.25 for $Zr(OBu)_4$), isopropanol, HCl, and $SmCl_3 \cdot 6H_2O$ was prepared (with molar ratio of 10/0.01/0.01 accordingly to the used amount of both alkoxides combined).

For both ZrO_2/SiO_2 mixtures the solution of water, Sm^{3+} , HCl, and solvent was added dropwise under stirring into the solution of alkoxides. A clear solution with a low viscosity was obtained; to get a viscous solution suitable for fibre pulling, the excess solvent was removed by evaporation under vacuum condition. Fibres were prepared by pulling the precursor sol into fibres by using a glass rod. The same precursor solution was also used to prepare relatively thick ($\sim 10 \mu m$) free-standing films suitable for the spectroscopic characteri-

zation (the precursor solution was poured into a Petri dish and left to gel and dry out for over a week; relatively thick pieces of a glass-like film were formed).

For the densification and release of carbon the as-prepared samples were heat-treated in air at temperatures ranging from 600°C to 1000°C. Indeed, it was earlier established [55] that the development of rare-earth-doped ZrO₂ nanocrystals inside the amorphous silica requires a thermal treatment at annealing temperatures reaching up to 1000 °C.

6.3 Results and discussion

The formation of separate crystalline ZrO₂ particles in an amorphous silica matrix was studied by Raman spectroscopy and XRD. The measured Raman spectra for the sample with concentration of 6.5% of ZrO₂ does not show any identifiable peaks of crystalline zirconia (Figure 14). The measured Raman spectra for the samples with concentration of 30% of ZrO₂ indicate that 800 °C is not a sufficient temperature for ZrO₂ crystallisation in this binary system. Identifiable spectra of the tetragonal phase of ZrO₂ appear only when the sample is annealed at least at 1000 °C (in accordance with reference [55]). The measured XRD spectrum (Figure 15) for such a sample also shows the formation of tetragonal phase and indicates that the formed crystallites are rather small, in the size range of couple of nanometres (no identifiable spectra have been obtained from the sample containing 6.5% of zirconia).

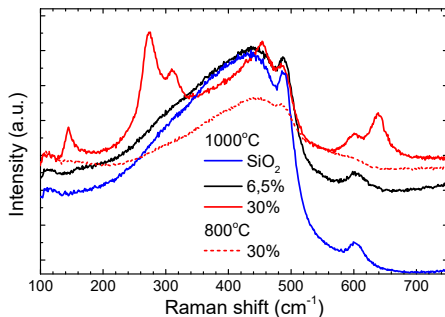


Figure 14: Raman spectra of silica-zirconia systems with different zirconia concentrations compared to the pure silica.

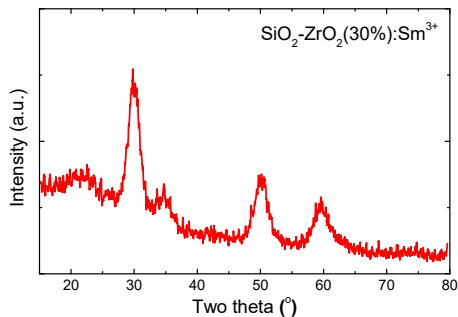


Figure 15: An XRD spectrum of silica-zirconia (30%) system annealed at 1000 °C.

The relatively broad PL bands of Sm³⁺ in combined PL spectra excited by 266 nm (Figure 16 and Figure 17) indicate that most of the PL is coming from ions situated in a glassy matrix for both zirconia concentrations [56-58]. The zirconia concentration increase to 30% enhances the Sm³⁺ emission compared to the defect emission. The intensity of Sm³⁺ PL increases with annealing up to

800 °C, but decreases with further annealing up to 1000 °C because at such temperatures the dopant ion might start to migrate to the surface.

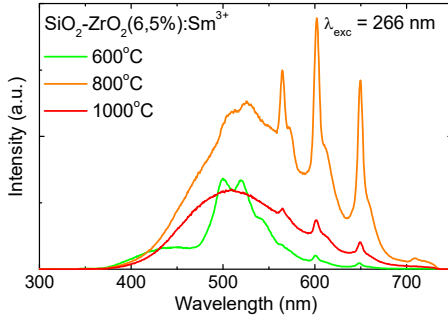


Figure 16: PL spectra of Sm^{3+} in silica-zirconia (6.5%) system, measured at room temperature with laser excitation at 266 nm.

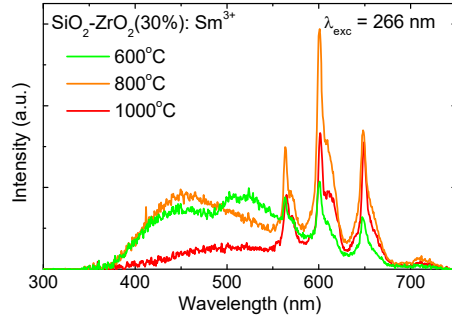


Figure 17: PL spectra of Sm^{3+} in silica-zirconia (30%) system, measured at room temperature with laser excitation at 266 nm.

6.4 Conclusions

Studied sol-gel method followed by a careful thermal treatment appears to be usable for preparation of rare-earth-doped $\text{SiO}_2/\text{ZrO}_2$ fibres. The structural analysis confirms the formation of zirconia nanocrystals. The dopants however tend not to be located in the ZrO_2 but rather in glassy silica surrounding. This is supported by the fact that the XRD and photoluminescence analyses suggest that only very small ZrO_2 crystallites are formed which naturally places most of the rare earth ions in disordered ZrO_2 and SiO_2 amorphous phase.

7. YSZ MICROTUBES

7.1 Introduction

Large-scale metal oxide materials, including ceramic tubes are prepared mostly from metal oxide powders through extrusion, followed by high-temperature sintering [59]. Unfortunately this mechanical processing approach becomes very difficult in the size range of a few hundred micrometres and below if well-defined geometry and mechanical and optical properties are needed. So, some sort of a “bottom-up” approach should be used to obtain a metal oxide material with both functional shape in the micro-scale and high structural homogeneity in the nano-scale, which are needed for materials with both good mechanical and optical properties. In this work, the mechanical drawing of material into a liquid thread combined with self-assembly processes of sol particles are used for preparation of yttrium-stabilized zirconia (YSZ) microtubes (Figure 18).

The microtubular shape of YSZ materials can give a lot of new possibilities for applications such as piping of liquids and gasses in microfluidics systems designed to be used under extreme conditions like elevated pressure and temperature (e.g. miniature reactors, lab-on-chip applications) [60], as an electrolyte material (YSZ has high ionic conductivity at elevated temperatures) for miniature microtubular solid oxide fuel cells (MT-SOFC) (for now having an average diameter of 1–4 mm) [61-63], for the use in gas sensing applications or as miniature plasma sources for applications requiring a good accuracy.

Doping of YSZ with optically active RE^{3+} ions enhances the material with additional luminescent properties and also allows to study with rather simple methods its structural evolution during the annealing process.

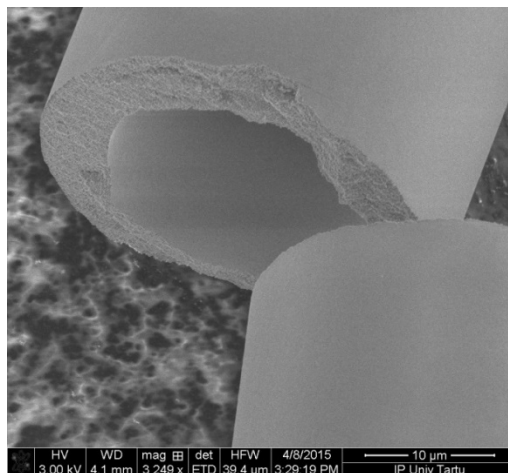


Figure 18: SEM image of a YSZ microtube.

7.2 Material preparation

For preparation of YSZ microtubes, a viscous sol with shear thinning viscoelastic properties is needed. To prepare such a sol, first a solution of water (5%), butanol, and Eu and Y nitrates is prepared with a ratio of 0.7 moles of water per 1 mole of alkoxide used. This solution is then added drop-wise under vigorous stirring to a $\text{Zr}(\text{OBU})_4$ and butanol solution. To transform the obtained homogeneous mixture into a honey-like viscous material suitable for the fibre pulling/pressing, almost all of the excess solvent is evacuated at 70 °C water bath, at 1–2 Torr vacuum conditions. The viscosity of the sol is now determined by the size of sol particles that is controlled by the alkoxide properties and by the rate of polymerization (the amount of added water).

To produce microtubes, initially a microfilament is formed that during the processes of gelling and phase separation hollows out to become a tube. Two methods have been used for filament drawing: the “glass rod method” and the “motorised jet pressing method”. The glass rod method is a rather simple technique where a glass rod is used to pull the prepared viscous sol into a fibre-like jet by a fast hand movement (Figure 19). The tubes prepared by this method have lengths of about 10–15 mm, typical outer diameters of 30–50 μm , and wall thicknesses of 10–15 μm . But the fibres made by this method are not always identical because the hand movements are not identical. The second method used for the initial fibre preparation, the motorised jet pressing method, is a more automated way to prepare fibres with identical parameters. In this case the viscous sol is pressed through a 200 μm nozzle with a constant speed (20–40 cm/s).

The solidification of the outer layer and the formation of the hollow core self-occurred during the first 15 minute period of the aging. The gelling process starts from the outer layer, forcing the solvent released during this process to remain inside the fibre. The sol particles self-assembly to form the walls of the tubes leading to the phase separation of solid gel and liquid solvent. The rest of the ageing period is needed to release organics as a vapour and also for the initial material densification. To further densify the material, to remove the organic residue, and to optimize the Eu^{3+} luminescence, the tubes were annealed at up to 1100 °C.

These tubes have excellent mechanical characteristics after heat treatment up to 700 °C, the Young's modulus and the tensile strength are in the range of 100–150 GPa and 400–600 MPa respectively, and they can withstand 1000 atm pressure inside the tubes [24].

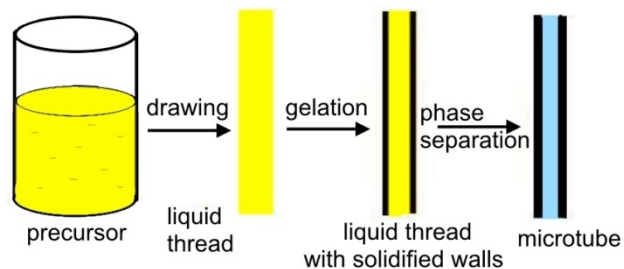


Figure 19: simplified overview of microtube formation

7.3 Results and discussion

The optical quality of the microtubes was investigated via light propagation in microtubes under an optical microscope. Both visible (532 nm) and UV (405 nm) laser light was used. One end of a microtube was illuminated with a strongly focused laser beam in order to couple the light into waveguiding modes, and the propagation of light was observed at the other end of the microtube, at a distance from the laser illumination (Figure 20).

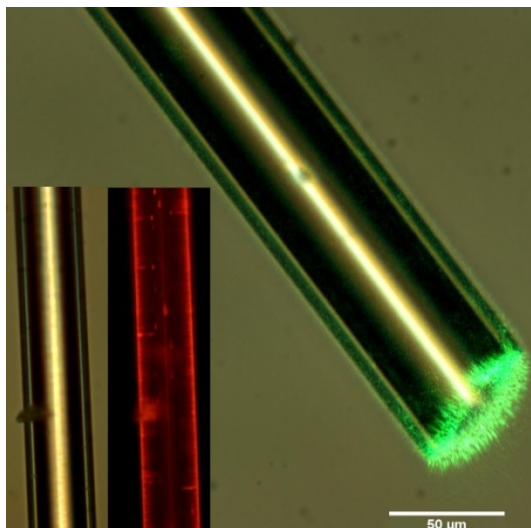


Figure 20: Propagation of green laser light (532 nm) through an YSZ microtube. Inset: optical micrographs of an Eu³⁺-doped YSZ microtube (left: illumination with white light; right: photoluminescence of Eu³⁺ excited by a 405 nm laser).

Due to a high amount of stabilizing dopants (8% Y and 1% Eu) we assume that the crystal structure of the microtubes remains tetragonal throughout the annealing temperature range. To check this assumption, Raman and XRD spectra were measured.

In the temperature range from 600 °C to 1100 °C the measured Raman spectra show only patterns assigned to tetragonal YSZ, and no identifiable peaks due to monoclinic phase are present. With the increase of annealing temperature a slight narrowing of the Raman peaks occurs due to the increase of the crystallite size [64, 65] (Figure 21).

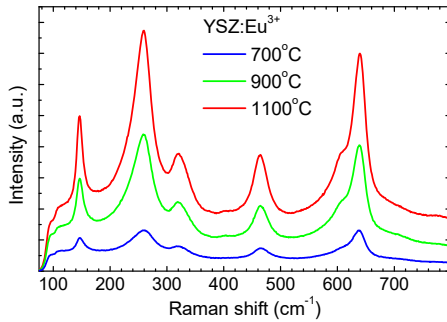


Figure 21: Raman spectra of YSZ:Eu³⁺ microtubes annealed at different temperatures.

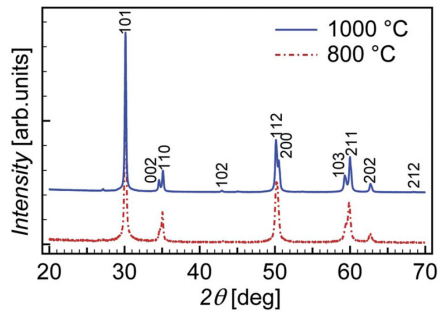


Figure 22: XRD spectra of YSZ:Eu³⁺ microtubes annealed at 800 °C and 1000 °C.

The measured X-ray diffraction pattern for powdered samples annealed at 800 °C shows that the tetragonal phase is prevalent, but a weak reflection from the monoclinic phase can also be seen for sample annealed at 1000 °C (Figure 22). The analysis of XRD peaks shows the growth of crystallites from 27(6) nm to 36(7) nm with the temperature increase.

The crystal structure of YSZ microtubes was further studied by the Eu³⁺ luminescence spectra. The luminescence of Eu³⁺ ions is very sensitive to the surrounding environment (matrix) and thus the corresponding spectra can be assigned to different crystal phases of the host material. Peaks at ~613 nm correspond to the monoclinic phase, and peaks at ~607 nm to tetragonal and cubic phases of ZrO₂ [66]. For microtubes annealed at 1100 °C, at least three distinguishable Eu³⁺ sites are observed.

A slight change in the excitation wavelength from 466 nm to 464 nm leads to two completely different spectra (Figure 23). The Eu centre corresponding to the excitation by 466 nm is labelled as Eu(1). The spectrum excited by 464 nm however, turns out to be a mixture of two different centres of Eu, as revealed by the time-resolved spectroscopy (Figure 24). The longer-living Eu centre is labelled as Eu(2), and the shorter-living centre as Eu(3). Several authors have reported either Eu(1) or Eu(2) type of Eu³⁺ spectra from ZrO₂ containing the

tetragonal phase [21, 67-69]. The shape of the Eu(3) spectrum suggest that the Eu^{3+} sites are located in less-ordered surrounding with lower symmetry, suggesting that the microtubes annealed at 1100 °C contain, in addition to the tetragonal phase, also some amount of the monoclinic phase, which can also be seen from the XRD spectra. The annealing temperature rise will grow the crystallites too big to be stabilized by the used amount of added yttrium.

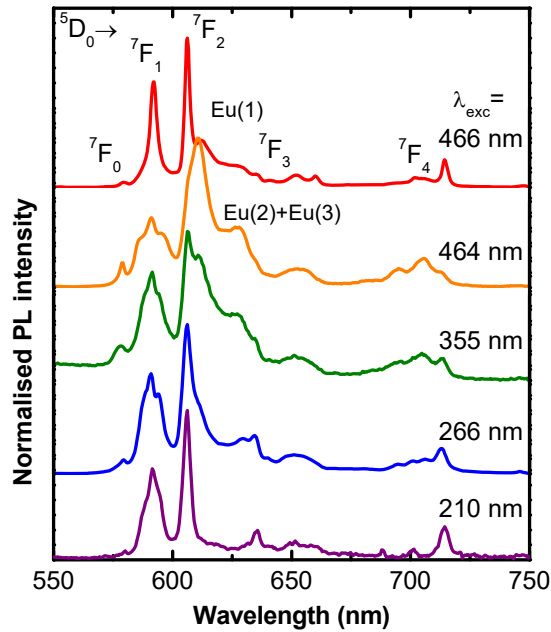


Figure 23: PL spectra of YSZ:Eu^{3+} microtubes annealed at 1100 °C, depending on the excitation wavelength.

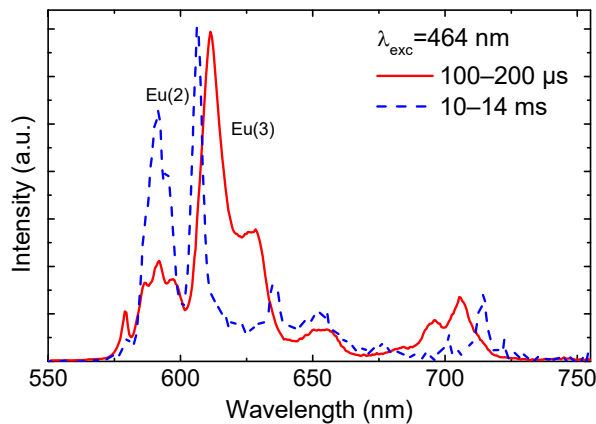


Figure 24: Time-resolved PL spectra of YSZ:Eu^{3+} microtubes annealed at 1100 °C, excited at 464 nm. The detection time window with respect to the laser pulse is indicated.

7.4 Applications

As noted before, YSZ has already been used for many different high-temperature applications, e.g. as a thermal barrier coating (TBC) or as an electrolyte material in solid oxide fuel cells (SOFC). To monitor the temperature of those complex and sometimes inaccessible structural elements, the non-contact fluorescence lifetime thermometry based on RE^{3+} dopant ions has been suggested [70-72]. The doping of an already functional oxide with luminescent activators enhances the material's functionality without any need for extra sensor layers.

To get a temperature reading from a Eu^{3+} lifetime measurement, a calibration curve of an average luminescence lifetime temperature dependence has to be measured (Figure 25). In reference to this curve the temperature value can be obtained. The testing of *in situ* non-contact fluorescence lifetime thermometry was carried out on a microtube annealed at 1000 °C, the tube was placed in an open-ended furnace. The Eu^{3+} luminescence was excited either by 466 nm or through the charge transfer absorption at 266 nm using a tuneable nanosecond laser. The Eu^{3+} decay curves were measured at the 606 nm peak using a photomultiplier operating in the photon counting regime and connected to a multi-channel analyser. The average sensitivity in the temperature range of 600 °C to 800 °C is ~ 0.5 C/%, which is on a par with that reported for conventional YSZ:Eu ceramics [71].

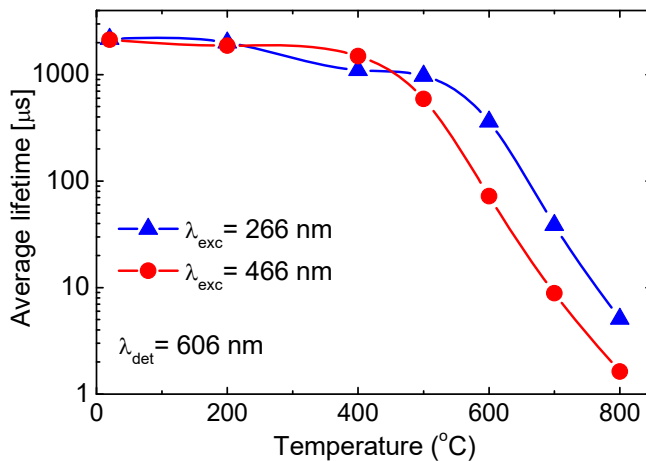


Figure 25: Temperature dependences of the Eu^{3+} fluorescence decay kinetics for two different excitation wavelengths (the solid curves are guides for the eye).

7.5 Conclusions

For optimizing the material densification (occurring via removal of residual organics and the oxide formation), temperatures of 700 °C to 800 °C are sufficient. At these temperatures the size of crystallites and the amount of stabilizing dopants fully stabilize the tetragonal phase. Annealing the YSZ microtube material at temperatures over 900 °C leads to the formation of small amounts of monoclinic phase. This can result in the formation of material defects, which affect the durability of microtubes at high temperatures and worsens the optical (wave guiding) properties of the material. If an application (like SOFC) needs higher working temperatures, then a larger amount of the stabilizing dopants should be used.

The fully stabilized zirconia microtubes have many possible applications like electrolytes in micro-SOFCs (YSZ has a high ion conductivity at elevated temperatures) and components of microfluidic systems (the obtained microtubes have excellent mechanical characteristics, and they can withstand 1000 atm pressure inside the tubes).

8. SUMMARY

Metal oxide mesostructures for optical applications

This PhD thesis is aimed at using sol-gel technique for forming a variety of metal oxide structures (mostly based on ZrO_2) and thorough characterization of the obtained materials. The focus is on the following applied aspects: (a) controlled morphology for better functionality, (b) phase composition and its stability and (c) optical/luminescence properties. Of special interest is the preparation of several quasi-1D microstructures – fibres, rolls, and tubes – which are rarely synthesized *via* soft chemical routes. The optical quality of some of the 1D structures is demonstrated by their light guiding capability. Although some materials had an intrinsic luminescence, trivalent rare-earth impurity ions were introduced during the synthesis for more robust luminescence functionality. Moreover, the fine structure analysis of the luminescence spectra complemented with XRD and Raman-scattering studies allowed monitoring of the structural evolution of the materials during the post-synthesis heat treatment period. Several aspects of the influence of high temperatures (>1000 °C), as well as the peculiarities of rare earth emission centres, have been clarified for studied oxide materials.

The more detailed results are summarized as follows:

- It was shown that after thermal treatment of pure ZrO_2 nanopowders beyond 1250 °C, a well-developed monoclinic structure is formed and a strong broadband intrinsic luminescence emerges around 490 nm. The emission has eminent thermoluminescence and afterglow properties, which are promising for phosphor and dosimetry applications.
- Luminescence properties of $ZrO_2:Sm^{3+}$ microrolls prepared by sol-gel process were studied. Doping of the material with Sm^{3+} fluorescent ions allowed optical monitoring of the nanoscale tetragonal-to-monoclinic phase transition during thermal annealing and assess its effects on the integrity of the microrolls.
- Sm-doped binary-oxide fibres of silica/zirconia solid solution were synthesized with an aim to obtain an active optical medium based on RE-doped crystalline nanoparticles distributed in a transparent glassy matrix. The formation of small tetragonal ZrO_2 nanocrystals was verified by XRD and Raman-scattering studies. The luminescence spectra indicate that the Sm^{3+} impurity ions are mostly located in a glassy environment, most probably in the SiO_2 matrix or at the phase boundaries.
- Luminescence properties of $Y_2O_3(8 \text{ mol}\%)-ZrO_2$ microtubular structures activated with Eu^{3+} ions were investigated and possible applications proposed. Optical studies indicated that the tetragonal phase is stabilized up to 900 °C. Observable dependence of the Eu^{3+} fluorescence lifetime in the range up to 800 °C enables its application in optical microthermometry for example in microfluidic systems under extreme conditions.

9. SUMMARY IN ESTONIAN

Metalloksiidsed mesostruktuurid optilisteks rakendusteks

Käesoleva doktoritöö eesmärgi – mõningate spetsiaalsete, peamiselt ZrO_2 põhiste, metalloksiidstruktuuride sool–geel meetodil valmistamise ja nende rakenduslikus plaanis oluliste aspektide nagu näiteks uudne funktsionaalne morfoloogia, faasikoostis ja selle stabiilsus ning optilised ja luminesentsomadused – saavutamiseks viidi läbi kompleksed uuringud. Peamist huvi pakkusid kvaasi ühedimensionaalsed mikrostruktuurid – fiibrid, rullid ja torud – mille süntees vedelkeemia meetodeil on võrdlemisi haruldane. Mõned saadud materjalid omandasid luminesentsomadused nominaalselt puhtal kujul, kuid stabiilsete luminesentsomaduste saavutamiseks lisandati materjalidele sünteesi käigus kolmevalentsete haruldaste muldmetallide ioone. Seejuures võimaldas lisandiluminesentsi spektraalse peenstruktuuri analüüs kombineerituna röntgen- ja raman-hajumise uuringutega jälgida materjalide struktuuri arengut sünteesijärgse termotöötuse käigus. Selgitati ka mitmeid aspekte temperatuuritöötuse ($>1000\text{ °C}$) mõju kohta materjalide kristallstruktuurile ja lisandtsentrite spektraalseid iseärasusi oksiidmaterjalides.

Uuringute olulisemad uued tulemused ja neist tehtud järeldused on järgnevad:

- Näidati, et nominaalselt lisandivabade ZrO_2 nanopulbrite termilisel töötusel temperatuuril 1250 °C või enam moodustus materjalis kaugelearenenud monokliinne kristallfaas, millega kaasnes intensiivne laia spektriga luminesentskiirgus 490 nm juures. Kiirgusele olid omased ka termoluminesents ja järelhelendus omadused, mis on perspektiivsed fosfoorides ja dosimeetrilistes rakendustes.
- Määrati kindlaks tingimused, mis viivad mikrorullide moodustumisele soolgeel protsessi käigus. Materjali dopeerimine fluorestseeruvate Sm^{3+} ioonidega lubas nanoskaalas optiliselt jälgida mikrorullide termotöötuse käigus toimuvat tetragonaalse kristallstruktuuri üleminekut monokliinseks.
- Sünteesiti samaariumi ioonidega dopeeritud SiO_2 - ZrO_2 segufiibrid, eesmärgiga realiseerida optiliselt aktiivne keskkond, kus Sm^{3+} ioonidega lisandatud ZrO_2 nanokristallid on dispergeeritud läbipaistvas klaasjas maatriksis. Termilise töötuse käigus tuvastati tetragonaalses faasis väikeste nanokristallide moodustumine röntgen-difraktsiooni ja raman-hajumise uuringute kaudu. Luminesentsispektrid viitasid Sm^{3+} lisandioonide asumisele valdavalt klaasjas ümbruses, oletatavalt SiO_2 maatriksis või faasiüleminekupiirkondades.
- Uuriti Eu^{3+} ioonidega dopeeritud $Y_2O_3(8\text{ mol}\%)-ZrO_2$ mikrotorujate struktuuride luminesentsomadusi ja sellest tulenevaid võimalikke rakendusi. Optiliste uuringute käigus tuvastati, et antud koostise juures on tetragonaalne faas stabiliseeritud kuni 900 °C -ni. Võimalik oli jälgida Eu^{3+} fluorestsentsi eluea süstemaatilist muutumist temperatuuri tõstmisel kuni 800 °C -ni. Nähtus on perspektiivne optilise mikrotermomeetria rakendustes eksteemsetel tingimustel (kõrge rõhk, temperatuur) töötavates mikrovedeliksüsteemides.

10. ACKNOWLEDGEMENTS

I would like to thank my supervisors dr. Ilmo Sildos, dr. Sven Lange and dr. Tanel Tätte for their support and help during the preparation of this work. I am thankful for valuable discussions with dr. Valter Kiisk and dr. Viktor Palm. Additionally I would like to thank Marko Part and dr. Martin Järvekülg for preparation of samples of microtubes and microrolls. Finally I would like to thank my parents and friends for their support.

This work was supported by the following agencies and foundations: Graduate School „Functional materials and technologies“ (European Social Fund project 1.2.0401.09-0079); “Mesosystems: Theory and Applications” (TK114); ERDF projects “Carbon Nanotube Reinforced Electrospun Nano-fibres and Yarns” (3.2.1101.12-0018) and “Efficient plasmonic absorbers for solar cells” (3.2.1101.12-0023).

11. REFERENCES

1. D. Koziej, A. Lauria, M. Niederberger. 25th anniversary article: metal oxide particles in materials science: addressing all length scales. *Advanced Materials*, 26 (2014), 235–257.
2. S. Sakka, Handbook of sol-gel science and technology; volume I: sol-gel processing. Kluwer Academic Publishers, 2005.
3. R. Reisfeld, T. Saraidarov. Innovative materials based on sol-gel technology. *Optical materials*, 28 (2006), 64–70.
4. J.D. Wright, N.A.J.M. Sommerdijk. Sol-gel materials: chemistry and applications. CRC press, 2000.
5. S. Sakka. Handbook of sol-gel science and technology; volume III: applications of sol-gel technology. Kluwer Academic Publishers, 2005.
6. R. Reisfeld, M. Zelner, A. Patra. Fluorescence study of zirconia films doped by Eu^{3+} , Tb^{3+} and Sm^{3+} and their comparison with silica films. *Journal of Alloys and Compounds*, 300–301 (2000), 147–151.
7. X. Zhao, D. Vanderbilt. Phonons and lattice dielectric properties of zirconia. *Physical Review B*, 65 (2002), 075105.
8. J. Gottmann, E.W. Kreutz. Pulsed laser deposition of alumina and zirconia thin films on polymers and glass as optical coatings. *Surface and Coatings Technology*, 116–119 (1999), 1189–1194.
9. N.Q. Minh. Solid oxide fuel cell technology – features and applications. *Solid State Ionics*, 174 (2004), 271–277.
10. N.P. Padture, M. Gell, E.H. Jordan. Thermal barrier coatings for gas-turbine engine applications. *Science*, 296 (2002), 280–284.
11. M. Zhou, A. Ahmad. Synthesis, processing and characterization of calcia-stabilized zirconia solid electrolytes for oxygen sensing applications. *Materials Research Bulletin*, 41 (2006), 690–696.
12. E. De la Rosa-Cruz, L.A. Diaz-Torres, P. Salas, D. Mendoza, J.M. Hernandez, V.M. Castano. Luminescence and thermoluminescence induced by gamma and UV-irradiation in pure and rare earth doped zirconium oxide. *Optical Materials*, 19 (2002), 195–199.
13. C. Piconi, G. Maccauro. Zirconia as a ceramic biomaterial. *Biomaterials*, 20 (1999), 1–25.
14. P.F. Manicone, P. Rossi Iommetti, L. Raffaelli. An overview of zirconia ceramics: Basic properties and clinical applications. *Journal of dentistry*, 35 (2007), 819–826.
15. V.E. Shukshin. Spectroscopic and lasing properties of disordered Yb^{3+} doped crystals. *Physics of wave phenomena*, 17, 3 (2009), 165–191.
16. E.V. Stefanovich, A.L. Shluger, C.R.A. Catlow. Theoretical study of the stabilization of cubic-phase ZrO_2 by impurities. *Physical Review B*, 49, 17 (1994), 11560–11571.
17. J.S. Hong, S.D. De la Torre, L. Gao, K. Miyamoto, H. Miyamoto. Synthesis and mechanical properties of $\text{ZrO}_2/\text{Al}_2\text{O}_3$ composites by spark plasma sintering. *Journal of Materials Science Letters*, 17 (1998), 1313–1315.
18. R.C. Garvie. The occurrence of metastable tetragonal zirconia as a crystallite size effect. *The Journal of Physical Chemistry*, 69, 4 (1965), 1238–1243.
19. M. Chatterjee, J. Ray, A. Chatterjee, D. Ganguli. High purity zirconia powders via wet chemical processing: a comparative study. *Ceramics International*, 18, 5 (1992), 337–342.

20. R. Piticescu, C. Monty, D. Millers. Hydrothermal synthesis of nanostructured zirconia materials: present state and future prospects. *Sensors and Actuators B*, 109 (2005), 102–106.
21. L. Chena, Y. Liu, Y. Li. Preparation and characterization of $\text{ZrO}_2\text{:Eu}^{3+}$ phosphors. *Journal of Alloys and Compounds*, 381 (2004), 266–271.
22. J. Joo, T. Yu, Y.W. Kim, H.M. Park, F. Wu, J.Z. Zhang, T. Hyeon. Multigram scale synthesis and characterization of monodisperse tetragonal zirconia nanocrystals. *Journal of American Chemical Society*, 125 (2003), 6553–6557.
23. D.M. Hausmann, R.G. Gordon. Surface morphology and crystallinity control in the atomic layer deposition (ALD) of hafnium and zirconium oxide thin films. *Journal of Crystal Growth*, 249 (2003), 251–261.
24. M. Part, K. Hanschmidt, J. Jögi, E. Rauwel, G.A. Seisenbaeva, V.G. Kessler, T. Tätte. Study of the curing mechanism of metal alkoxide liquid threads for the synthesis of metal oxide fibers and microtubes. *RSC Advances*, 4 (2014), 12545–12554.
25. C. Zhang, J. Lin. Defect-related luminescent materials: synthesis, emission properties and applications. *Chemical Society Reviews*, 41 (2012), 7938–7961.
26. P. Tanner. Some misconceptions concerning the electronic spectra of tri-positive europium and cerium. *Chemical Society Reviews*, 42, 12 (2013), 5090–5101.
27. R. Reisfeld, E. Zigansky, M. Gaft. Europium probe for estimation of site symmetry in glass films, glasses and crystals. *Molecular Physics*, 102, 11–12 (2004), 1319–1330.
28. S.F. Wang, F. Gu, M.K. Lü, Z.S. Yang, G.J. Zhou, H.P. Zhang, Y.Y. Zhou, S.M. Wang. Structure evolution and photoluminescence properties of $\text{ZrO}_2\text{:Eu}^{3+}$ nanocrystals. *Optical materials*, 28 (2006), 1222–1226.
29. M. Järvekülg, R. Välbe, J. Jögi, A. Salundi, T. Kangur, V. Reedo, J. Kalda, U. Mäeorg, A. Lõhmus, A.E. Romanov. A sol-gel approach to self-formation of microtubular structures from metal alkoxide gel films. *Physica Status Solidi A*, 209, 12 (2012), 2481–2486.
30. M. Niederberger, N. Pinna. Metal oxide nanoparticles in organic solvents. Springer, 2009.
31. N.Y. Turova, E.P. Turevskaya, V.G. Kessler, M.I. Yanovskaya. The chemistry of metal alkoxides. Kluwer Academic Publishers, 2002.
32. D.C. Bradley, R.C. Mehrota, I.P. Rothwell, A. Singh. Alkoxo and aryloxo derivatives of metals. Elsevier, 2001.
33. V.G. Kessler. The chemistry behind the sol-gel synthesis of complex oxide nanoparticles for bio-imaging applications. *Journal of Sol-Gel Science and Technology*, 51 (2009), 264–271.
34. H.K. Schmidt. Relevance of sol-gel methods for synthesis of fine particles. *KONA*, 14 (1996), 92–103.
35. G.I. Spijksma, G.A. Seisenbaeva, A. Fischer, H.J.M. Bouwmeester, D.H.A. Blank, V.G. Kessler. The molecular composition of non-modified and acac-modified propoxide and butoxide precursors of zirconium and hafnium dioxides. *Journal of Sol-Gel Science and Technology*, 51 (2009), 10–22.
36. T. Saegussa, Y. Chujo. An organic/inorganic hybrid polymer. *Journal of Macromolecular Science: Pure and Applied Chemistry*, 27 (1990), 1603–1612.
37. F. Kirkbir, H. Murata, D. Meyers, S.R. Chaudhuri. Drying large monolithic aerogels between atmospheric and supercritical pressures. *Journal of Sol-Gel Science and Technology*, 13 (1998), 311–316.

38. A. Krell, T. Hutzler, J. Klimke, A. Potthoff. Fine-grained transparent spinel windows by the processing of different nanopowders. *Journal of the American Ceramic Society*, 93 (2010), 2656–2666.
39. J.B. MacCesney. Advanced ceramics III: sol-gel processing of optical waveguides. Springer. 1990.
40. J.M. Carvalho, L.C.V. Rodrigues, M.C.F.C. Felinto, L.A.O. Nunes, J. Hölsä, H.F. Brito. Structure-property relationship of luminescent zirconia nanomaterials obtained by sol-gel method. *Journal of Materials Science*, 50 (2015), 873–881.
41. V. Kiisk, S. Lange, K. Utt, T. Tätte, H. Mändar, I. Sildos. Photoluminescence of sol-gel-prepared hafnia. *Physica B*, 405 (2010), 758–762.
42. Y. Cong, B. Li, B. Lei, W. Li. Long lasting phosphorescent properties of Ti doped ZrO₂. *Journal of Luminescence*, 126 (2007), 822–826.
43. D.A. Pejakovic. Studies of the phosphorescence of polycrystalline hafnia. *Journal of Luminescence*, 130 (2010), 1048–1054.
44. C. Bettinali, G. Ferraresso, J.W. Manconi. Thermoluminescence of ZrO₂. *The Journal of Chemical Physics*, 50 (1969), 3957–3961.
45. Y. Cong, B. Li, S. Yue, D. Fan. Effect of oxygen vacancy on phase transition and photoluminescence properties of nanocrystalline zirconia synthesized by the one-pot reaction. *The Journal of Physical Chemistry C*, 113 (2009), 13974–13978.
46. J.M. Carvalho, L.C.V. Rodrigues, J. Hölsä, M. Lastusaari, L.A.O. Nunes, M.C.F.C. Felinto, O.L. Malta, H.F. Brito. Influence of titanium and lutetium on the persistent luminescence of ZrO₂. *Optical Materials Express*, 2 (2012), 331–340.
47. Z. Wang, J. Zhang, G. Zheng, Y. Liu, Y. Zhao. The unusual variations of photoluminescence and afterglow properties in monoclinic ZrO₂ by annealing. *Journal of Luminescence*, 132 (2012), 2817–2821.
48. H. Wen-Ching, S. Ching-Shen. UV induced thermoluminescence in ZrO₂ doped by Er₂O₃. *Journal of Physics D: Applied Physics*, 27 (1994), 1763–1768.
49. T. Rivera Montalvo, L. Olvera Tenorio, J. Azorin Nieto, A. Campero Celis, C. Velquez Ordonez, R. Sosa Fonseca. Thermoluminescence and optical characteristics of ZrO₂ powder as a TL dosimeter. *Radiation Effects & Defects in Solids*, 159 (2004), 645–649.
50. Q. le Masne de Chermont, C. Chaneac, J. Seguin, F. Pelle, S. Maitrejean, J-P. Jolivet, D. Gourier, M. Bessodes, D. Scherman. Nanoparticles with near-infrared persistent luminescence for in vivo imaging. *Proceedings of the National Academy of Sciences of the United States of America*, 104, 22 (2007), 9266–9271.
51. J. Jõgi, M. Järvekülg, J. Kalda, A. Salundi, V. Reedo, A. Lõhmus. Simulation of cracking of metal alkoxide gel film formed on viscous precursor layer using a spring-block model. *A Letters Journal Exploring the Frontiers of Physics*, 95 (2011), 64005.
52. S. Lange, I. Sildos, M. Hartmanova, J. Aarik, V. Kiisk. Luminescence properties of Sm³⁺ doped polycrystalline ZrO₂. *Journal of Non-Crystalline Solids*, 354 (2008), 4380–4382.
53. E. De la Rosa, L.A. Diaz-Torres, P. Salas, R.A. Rodrigues, C. Angeles. Temperature effect in the crystallite size and the photoluminescence of nanocrystalline ZrO₂:Sm³⁺ phosphor. *Proceedings of SPIE*, 5510 (2004), 57–67.
54. A. Gaudon, F. Lallet, A. Bouille, A. Lecomte, B. Soulestin. From amorphous phase separations to nanostructured materials in sol-gel derived ZrO₂:Eu³⁺/SiO₂ and ZnO/SiO₂ composites. *Journal of Non-Crystalline Solids*, 352 (2006), 2152–2158.

55. G. Brasse, C. Restoin, J-L. Auguste, S. Hautreux, J-M. Blondy, A. Lecomte, F. Sandoz, C. Pedrido. Nanoscaled optical fibre obtained by the sol-gel process in the $\text{SiO}_2\text{-ZrO}_2$ system doped with rare earth ions. *Optical Materials*, 31 (2009), 765–768.
56. A. Herrmann, S. Kuhn, M. Tiegel, C. Rüssel, J. Körner, D. Klöpfel, J. Hein, M.C. Kaluza. Structure and fluorescence properties of ternary aluminosilicate glasses doped with samarium and europium. *Journal of Materials Chemistry C*, 2 (2014), 4328.
57. Y. Zhang, C. Lu, L. Sun, Z. Xu, Y. Ni. Influence of Sm_2O_3 on the crystallization and luminescence properties of boroaluminosilicate glasses. *Materials Research Bulletin*, 44 (2009), 179–183.
58. S. Buddhudu, M. Morita, S. Murakami, D. Rau. Temperature-dependent luminescence and energy transfer in europium and rare earth codoped nanostructured xerogel and sol-gel silica glasses. *Journal of Luminescence*, 83–84 (1999), 199–203.
59. E.A. Barringer, H.K. Bowen. Formation, packing and sintering of monodisperse TiO_2 powders. *Journal of American Ceramic Society*, 65 (1982), 199–203.
60. P. Abgrall, A-M. Gue. Lab-on-chip technologies: making a microfluidic network and coupling It into a complete microsystem - a review. *Journal of Micromechanics and Microengineering*, 17 (2007), R15-R49.
61. M.H.D. Othman, N. Droushiotis, Z. Wu, G. Kelsall, K. Li. High-performance, anode-supported, microtubular SOFC prepared from single-step-fabricated, dual-layer hollow fibers. *Advanced Materials*, 23 (2011), 2480–2483.
62. V. Lawlor. Review of the micro-tubular solid oxide fuel cell (part II: cell design issues and research activities). *Journal of Power Sources*, 240, 421–441.
63. K.S. Howe, G.J. Thompson, K. Kendall. Micro-tubular solid oxide fuel cells and stacks. *Journal of Power Sources*, 196 (2011), 1677–1686.
64. D. Gazzoli, G. Mattei, M. Valigi. Raman and X-ray investigations of the incorporation of Ca^{2+} and Cd^{2+} in the ZrO_2 structure. *Journal of Raman Spectroscopy*, 38 (2007), 824–831.
65. E. Fernandez Lopez, V. Sanchez Escribano, M. Panizza, M.M. Carnasciali, G. Busca. Vibrational and Electronic Spectroscopic Properties of Zirconia Powders. *Journal of Materials Chemistry*, 11 (2001), 1891–1897.
66. K. Smits, L. Grigorjeva, D. Millers, A. sarkovskis, A. Opalinska, J. D. Fidelus, W. Lojkowski. Europium doped zirconia luminescence. *Optical Materials*, 32 (2010), 827–831.
67. A. Speghini, M. Bettinelli. Preparation, structural characterization, and luminescence properties of Eu^{3+} doped nanocrystalline ZrO_2 . *Journal of Materials Research*, 20, 10 (2005).
68. J. Liao, D. Zhou, B. Yang, R. Liu, Q. Zhang. Sol-gel preparation and photoluminescence properties of tetragonal $\text{ZrO}_2\text{:Y}^{3+}$, Eu^{3+} Nanophosphors. *Optical Materials*, 35 (2012), 274–279.
69. M.R.N. Soares, C. Nico, M. Peres, N. Ferreira, A.J.S. Fernandes, T. Monteiro, M. Costa. Structural and optical properties of europium doped zirconia single crystals fibers grown by laser floating zone. *Journal of Applied Physics*, 109, 1 (2011).
70. M.D. Chambers, D.R. Clarke. Effect of long term, high temperature aging on luminescence from Eu-doped YSZ thermal barrier coatings. *Surface and Coatings Technology*, 201 (2006), 3942–3946.
71. D.R. Clarke, M.D. Chambers. Doped oxides for high-temperature luminescence and lifetime thermometry. *The Annual Review of Materials Research* (2009), 325–329.
72. M.M. Gentleman, D.R. Clarke. Concepts for luminescence sensing of thermal barrier coatings. *Surface and Coatings Technology*, 188–189 (2004), 93–100.

12. PUBLICATIONS

CURRICULUM VITAE

Name: Kathriin Utt
Date of birth: 16.03.1986
Nationality: Estonian
E-mail: kathriin@ut.ee

Education:

2009–2011 University of Tartu MSc (materials science)
2005–2009 University of Tartu BSc (materials science)
1993–2005 Rapla Vesiroosi Gymnasium

Career:

04.2011–12.2015 University of Tartu, Institute of Physics, laboratory assistant

List of publications:

Publications included in the thesis:

1. L. Puust, V. Kiisk, **K. Utt**, H. Mändar, I. Sildos, (2014). Afterglow and thermoluminescence of ZrO₂ nanopowders. *Central European Journal of Physics*, 12(6), 415–420.
2. **K. Utt**, S. Lange, M. Järvekülg, H. Mändar, P. Kanarjov, I. Sildos, (2010). Structure and optical properties of Sm-doped ZrO₂ microrolls. *Optical Materials*, 32(8), 823–826.
3. **K. Utt**, M. Part, T. Tätte, V. Kiisk, M. G. Brik, A. A. Chaykin, I. Sildos, (2014). Spectroscopic properties of Eu-doped Y-stabilized ZrO₂ microtubes. *Journal of Luminescence*, 125–128.
4. T. Tätte, M. Part, R. Talviste, K. Hanschmidt, **K. Utt**, U. Mäeorg, I. Jõgi, V. Kiisk, H. Mändar, G. Nurk, P. Rauwel, (2014). Yttria stabilized zirconia microtubes for microfluidics under extreme conditions. *RSC Advances*, 4(34), 17413–17419.

Publications not related to the thesis:

1. Kiisk, L. Puust, **K. Utt**, A. Maaros, H. Mändar, E. Viviani, F. Piccinelli, R. Saar, U. Joost, I. Sildos, (2016). Photo-, thermo- and optically stimulated luminescence of monoclinic zirconia. *Journal of Luminescence*, 174, 49–55.
2. M. Eltermann, K. Utt, S. Lange, R. Jaaniso, (2016). Sm³⁺ doped TiO₂ as optical oxygen sensor material. *Optical Materials*, 51, 24–30.
3. Kiisk, A. Tamm, **K. Utt**, J. Kozlova, H. Mändar, L. Puust, J. Aarik, I. Sildos, (2015). Photoluminescence of atomic layer deposited ZrO₂:Dy³⁺ thin films. *Thin Solid Films*, 583, 70–75.
4. T. Dedova, I. Gromyko, M. Krunks, V. Mikli, M. Grossberg, I. Sildos, I.; **K. Utt**, R. Vessart, T. Unt, (2015). Spray pyrolysis deposition and characterization of highly c-axis orientated hexagonal ZnS nanorod crystals. *Crystal research and technology*, 50(1), 82–95.

5. D. Klauson, I. Gromyko, T. Dedova, N. Pronina, M. Krichevskaya, O. Budarnaja, I. Oja Acik, O. Volobujeva, I. Sildos, **K. Utt**, (2015). Study of photocatalytic activity of zinc oxide nanoneedles, nanorods, pyramids and hierarchical structures obtained by spray pyrolysis. *Materials Science in Semiconductor Processing*, 31, 315–324.
6. T. Dedova, M. Krunks, I. Gromyko, V. Mikli, I. Sildos, **K. Utt**, T. Unt, (2014). Effect of Zn:S molar ratio in solution on properties of ZnS thin films and formation of ZnS nanorods by spray pyrolysis. *Physica Status Solidi A – Applications and Materials Science*, 211(2), 514–521.
7. U. Joost, A. Saarva, M. Visnapuu, E. Nõmmiste, **K. Utt**, R. Saar, V. Kisand, (2014). Purification of titania nanoparticle thin films: Triviality or a challenge? *Ceramics International*, 40(5), 7125–7132.
8. U. Joost, R. Pärna, M. Lembinen, **K. Utt**, I. Kink, M. Visnapuu, V. Kisand, (2013). Heat treatment and substrate dependent properties of titania thin films with high copper loading. *Physica Status Solidi A – Applications and Materials Science*, 210(6), 1201–1212.
9. Kiisk, S. Lange, **K. Utt**, T. Tätte, H. Mändar, I. Sildos, (2010). Photoluminescence of sol-gel-prepared hafnia. *Physica B: Condensed Matter*, 405, 758–762.

ELULOOKIRJELDUS

Nimi: Kathriin Utt
Sünniaeg: 16.03.1986
Kodakondsus: Eesti
E-post: kathriin@ut.ee

Haridus:

2009–2011 Tartu Ülikool, Tehnikateaduste magister (materjaliteadus)
2005–2009 Tartu Ülikool, Tehnikateaduste bakalaureus
(materjaliteadus)
1993–2005 Rapla Vesiroosi Gümnaasium

Töökogemus:

04.2011–12.1015 Tartu Ülikooli Füüsika Instituut, laborant

Publikatsioonide loetelu:

Publikatsioonid doktoritöös:

1. L. Puust, V. Kiisk, **K. Utt**, H. Mändar, I. Sildos, (2014). Afterglow and thermoluminescence of ZrO₂ nanopowders. *Central European Journal of Physics*, 12(6), 415–420.
2. **K. Utt**, S. Lange, M. Järvekülg, H. Mändar, P. Kanarjov, I. Sildos, (2010). Structure and optical properties of Sm-doped ZrO₂ microrolls. *Optical Materials*, 32(8), 823–826.
3. **K. Utt**, M. Part, T. Tätte, V. Kiisk, M. G. Brik, A. A. Chaykin, I. Sildos, (2014). Spectroscopic properties of Eu-doped Y-stabilized ZrO₂ microtubes. *Journal of Luminescence*, 125–128.
4. T. Tätte, M. Part, R. Talviste, K. Hanschmidt, **K. Utt**, U. Mäeorg, I. Jõgi, V. Kiisk, H. Mändar, G. Nurk, P. Rauwel, (2014). Yttria stabilized zirconia microtubes for microfluidics under extreme conditions. *RSC Advances*, 4(34), 17413–17419.

Publikatsioonid, mis ei ole doktoritööga seotud:

1. V. Kiisk, L. Puust, **K. Utt**, A. Maaros, H. Mändar, E. Viviani, F. Piccinelli, R. Saar, U. Joost, I. Sildos, (2016). Photo-, thermo- and optically stimulated luminescence of monoclinic zirconia. *Journal of Luminescence*, 174, 49–55.
2. M. Eltermann, K. Utt, S. Lange, R. Jaaniso, (2016). Sm³⁺ doped TiO₂ as optical oxygen sensor material. *Optical Materials*, 51, 24–30.
3. V. Kiisk, A. Tamm, **K. Utt**, J. Kozlova, H. Mändar, L. Puust, J. Aarik, I. Sildos, (2015). Photoluminescence of atomic layer deposited ZrO₂:Dy³⁺ thin films. *Thin Solid Films*, 583, 70–75.
4. T. Dedova, I. Gromyko, M. Krunk, V. Mikli, M. Grossberg, I. Sildos, I.; **K. Utt**, R. Vessart, T. Unt, (2015). Spray pyrolysis deposition and characteri-

- zation of highly c-axis orientated hexagonal ZnS nanorod crystals. *Crystal research and technology*, 50(1), 82–95.
5. D. Klauson, I. Gromyko, T. Dedova, N. Pronina, M. Krichevskaya, O. Budarnaja, I. Oja Acik, O. Volobujeva, I. Sildos, **K. Utt**, (2015). Study of photocatalytic activity of zinc oxide nanoneedles, nanorods, pyramids and hierarchical structures obtained by spray pyrolysis. *Materials Science in Semiconductor Processing*, 31, 315–324.
 6. T. Dedova, M. Krunks, I. Gromyko, V. Mikli, I. Sildos, **K. Utt**, T. Unt, (2014). Effect of Zn:S molar ratio in solution on properties of ZnS thin films and formation of ZnS nanorods by spray pyrolysis. *Physica Status Solidi A – Applications and Materials Science*, 211(2), 514–521.
 7. U. Joost, A. Saarva, M. Visnapuu, E. Nõmmiste, **K. Utt**, R. Saar, V. Kisand, (2014). Purification of titania nanoparticle thin films: Triviality or a challenge? *Ceramics International*, 40(5), 7125–7132.
 8. U. Joost, R. Pärna, M. Lembinen, **K. Utt**, I. Kink, M. Visnapuu, V. Kisand, (2013). Heat treatment and substrate dependent properties of titania thin films with high copper loading. *Physica Status Solidi A – Applications and Materials Science*, 210(6), 1201–1212.
 9. V. Kiisk, S. Lange, **K. Utt**, T. Tätte, H. Mändar, I. Sildos, (2010). Photoluminescence of sol-gel-prepared hafnia. *Physica B: Condensed Matter*, 405, 758–762.

DISSERTATIONES SCIENTIAE MATERIALIS UNIVERSITATIS TARTUENSIS

1. **Martin Järvekülg.** Tubular microstructures by Hf-, Zr- and Ti-butoxide gel sheet rolling. Tartu, 2011, 112 p.
2. **Sergei Vlassov.** Investigation of nanoscale interactions and mechanical properties of nanostructures using quartz tuning fork based real-time measurements. Tartu, 2011, 171 p.
3. **Margus Kodu.** Pulsed Laser Deposition of Magnesium Oxide and Barium Ternary Oxides for Plasma Display Protective Layers. Tartu, 2011, 89 p.
4. **Rainer Pärna.** Surface studies of some oxide films. Tartu, 2011, 129 p.
5. **Jevgeni Šulga.** Self-assembly and interaction of nanostructures. Tartu, 2011, 114 p.
6. **Wojciech Kuznik.** Quantum-chemical computer simulations of the linear and non-linear optical properties of pyrazoloquinoline and dicyanopyrazine derivatives. Tartu, 2012, 89 p.
7. **Leonid Dorogin.** Structural and tribological properties of zero- and one-dimensional nanocrystals. Tartu, 2012, 193 p.
8. **Viljar Palmre.** Fabrication and characterization of microporous carbon-based electroactive polymer actuators. Tartu, 2012, 99 p.
9. **Madis Paalo.** Synthesis of CNT-metal oxide nanocomposites: sol-gel process, rheology, structural and functional properties. Tartu, 2014, 175 p.
10. **Raul Välbe.** Development of ionic liquid composites by sol-gel method for elaboration of industrial nano- and microstructures. Tartu, 2014, 97 p.
11. **Urmas Joost.** Impurity and preparation dependent properties of titania thin films. Tartu, 2014, 155 p.
12. **Madis Umalas.** Application of sol-gel technology for production of ceramic nanocomposites and functional coatings. Tartu, 2015, 136 p.
13. **Elena Samsonova.** Energy transfer probe as a tool to study morphological and structural origins of fluorescence quenching in rare-earth doped nanophosphors. Tartu, 2015, 114 p.
14. **Jay Mondal.** Novel Corrosion Protective Nanostructured Composite Coatings. Tartu, 2016, 104 p.